

# Deep Computerized Adaptive Testing

Jiguang Li\*, Robert Gibbons† and Veronika Ročková‡

March 10, 2025

## Abstract

Computerized adaptive tests (CATs) play a crucial role in educational assessment and diagnostic screening in behavioral health. Unlike traditional linear tests that administer a fixed set of pre-assembled items, CATs adaptively tailor the test to an examinee’s latent trait level by selecting a smaller subset of items based on their previous responses. Existing CAT applications predominantly rely on item response theory (IRT) models with a single latent variable, a choice driven by both conceptual simplicity and computational feasibility. However, many real-world item response datasets exhibit complex, multi-factor structures, limiting the applicability of CATs in broader settings. In this work, we develop a novel CAT system that incorporates multivariate latent traits, building on recent advances in Bayesian sparse multivariate IRT [1]. Our approach leverages direct sampling from the latent factor posterior distributions, significantly accelerating existing information-theoretic item selection criteria by eliminating the need for computationally intensive Markov Chain Monte Carlo (MCMC) simulations. Recognizing the potential suboptimality of existing item selection rules which are often based on myopic one-step-lookahead optimization of some information-theoretic criterion, we propose a double deep Q-learning algorithm to learn an optimal item selection policy. Through simulation and real-data studies, we demonstrate that our approach not only accelerates existing item selection methods but also highlights the potential of reinforcement learning in CATs. Notably, our Q-learning-based strategy consistently achieves the fastest posterior variance reduction, leading to earlier test termination. In finite-horizon settings, it also yields final posterior distributions that more closely approximate the oracle posterior distribution—the posterior that would be obtained if test takers had responded to all items in the item bank.

*Keywords:* Reinforcement Learning; Multidimensional Item Response Theory; Adaptive Data Collection; Deep Q-Learning;

---

\*Jiguang Li is a 3<sup>rd</sup>-year doctoral student in Econometrics and Statistics at the Booth School of Business of the University of Chicago

†Robert Gibbons is the Blum-Reise Professor of Statistics at the University of Chicago

‡Veronika Ročková is the Bruce Lindsay Professor of Econometrics and Statistics in the Wallman Society of Fellows

# 1 Introduction

Computerized adaptive testing (CAT) has transformed modern assessment in education and behavioral health by tailoring test content to individual examinees in real time. Unlike traditional linear tests, which present a fixed set of items to all test-takers, CAT dynamically selects questions from a large item bank based on an examinee’s prior responses. This adaptivity enhances both the efficiency and precision of ability estimation by continuously presenting items that are neither too easy nor too difficult [2]. By focusing on items that provide the most information, CAT reduces the number of questions needed to reach an accurate assessment, enabling earlier test termination without sacrificing measurement accuracy. This efficiency is especially valuable in high-stakes diagnostic settings, such as clinical psychology, where CAT can serve as an alternative to in-person evaluations, helping to expand access to assessments in resource-limited environments [3].

CAT frameworks typically consist of two key components: a psychometric model based on item response theory (IRT) [4] and an online item selection rule that maximizes an information-theoretic criterion (e.g., [5, 6]). Given an item response dataset, statisticians first fit an IRT model to estimate item characteristic parameters, which capture properties such as discrimination and difficulty of each item. These parameters provide valuable psychometric insights that guide online item selection for future examinees. The efficiency of a CAT system can be assessed by the number of items required to estimate an examinee’s latent traits with sufficient precision, typically defined as reducing uncertainty below a predetermined threshold.

The psychometric models underlying many CAT frameworks can be overly simplified. Most implementations assume an IRT model with a single latent variable, primarily due to the computational challenges of rapid online item selection in multi-factor latent spaces. However, this assumption is often questionable in real-world item response datasets, such as in behavioral health assessments [7], where items can span multiple domains. As a result,

it can lead to biased estimates of item parameters and latent traits, limiting the adaptivity of current CAT systems in many assessment settings. While fitting a multidimensional IRT (MIRT) model is conceptually straightforward, updating high-dimensional latent trait estimates while optimizing item selection criteria in real time remain challenging.

Although numerous item selection rules have been proposed in the CAT literature, they all rely on one-step lookahead greedy optimization of an information-theoretic criterion [6, 8, 9, 10]. Despite their ease of implementation, these selection rules are inherently myopic and suboptimal, as they fail to account for future decisions. For example, existing methods tend to favor items with high discrimination parameters [11]. However, CAT researchers also recommend reserving highly discriminating items for the later stages of testing to improve efficiency [12]. Integrating heuristic guidance into existing selection rules still remains nontrivial.

To address these critical challenges, we propose a novel deep CAT system that integrates a flexible Bayesian MIRT model with a non-myopic online item selection policy, guided by reinforcement learning (RL) principles [13]. Leveraging recent advancements in Bayesian sparse MIRT [1], our framework seamlessly accommodates multiple latent factors with complex loading structures, while maintaining scalability in both the number of items and factors. To learn the optimal item selection policy prioritizing the assessment of target factors, we draw on contemporary RL methodologies [13] and introduce a general double deep Q-learning algorithm [14, 15]. This algorithm trains a deep Q-network offline using only item parameter estimates which is subsequently deployed online to select optimal items based on the current multivariate latent factor posterior distribution. When the test terminates, our framework robustly characterizes the full latent factor posterior distributions rather than providing only a point estimate.

A primary contribution of our work is the significant improvement in computational scalability for online item selection, allowing it to scale efficiently with both the number

of items and latent factors. This speedup is achieved by directly sampling latent factor posterior distributions [1, 16, 17] in parallel, eliminating the need for computationally intensive Markov Chain Monte Carlo (MCMC) simulations. Notably, this advancement extends beyond our proposed deep Q-learning framework and can accelerate any existing CAT item selection algorithms that requires latent factor posterior sampling.

Another critical advancement in our work is the integration of CAT within a reinforcement learning framework. This is motivated by both the practical need to prioritize the accurate assessment of the primary factors of interest in the presence of high-dimensional latent structures, as well as by the well-documented limitations of existing greedy approaches in sequential decision-makings [13, 18]. The sequential nature of CAT aligns naturally with deep Q-learning methods, which have demonstrated remarkable success across diverse application domains [14, 19, 20, 21]. However, designing network architectures for CAT systems presents unique challenges, as they require both minimal online item selection time and careful parametrization of latent factor posterior distributions.

Our work aligns with the emerging research trend of framing traditional statistical sequential decision-making problems as optimal policy learning tasks [22]. In Bayesian adaptive design [23], a common approach is to select the next experiment to maximize expected information gain [24], while deep neural networks have demonstrated success in learning non-myopic policies that optimize cumulative information gain [25]. Similarly, Bayesian optimization often relies on myopic one-step strategies like expected improvement [26] and upper confidence bound [27], while more recent methods such as Entropy Search [28] and multi-step lookahead [29] have improved long-term performance. Our work contributes to these advancements by providing a principled approach to mitigating myopic decision-making in cognitive and behavioral assessments.

The remainder of the paper is organized as follows. Section 2 contextualizes our deep CAT framework using a cognitively complex item bank from a recent clinical study [7].

Section 3 reviews existing information-theoretic item selection methods and outlines the necessity to reformulating CAT as a reinforcement learning task. Section 4 presents a general strategy for sequentially sampling latent factor posterior distributions, eliminating the need for MCMC simulations. Section 5 details our reinforcement learning approach, including the neural network architecture and double Q-learning algorithm. Finally, Section 6 evaluates our method through simulations and real data experiments.

## 2 Adaptive High-Dimensional Cognitive Assessment

Our proposed deep CAT system is motivated by the growing need for adaptive cognitive assessment in high-dimensional latent spaces. Cognitive impairment, particularly Alzheimer’s dementia (AD), is a major public health challenge, affecting 6.9 million individuals in the U.S. in 2024 [30]. Early detection of mild cognitive impairment (MCI), a precursor to AD, is crucial for slowing disease progression and improving patient outcomes [31]. However, traditional neuropsychological assessments are costly, time-consuming, and impractical for frequent use, underscoring the need for more efficient and scalable assessment methods.

Recently, pCAT-COG, the first computerized adaptive test (CAT) item bank based on MIRT for cognitive assessment, demonstrated its potential as an alternative to clinician-administered evaluations [7]. The data was collected from 730 participants. After careful item calibration and model selections, the final item bank consisted of  $J = 57$  items covering five cognitive subdomains: episodic memory, working memory, executive function, semantic memory, and processing speed. Since each item comprised three related tasks, we used a binary score, where 1 indicates correct answers on all tasks for our analysis.

Following [7], we fit a six-factor bifactor model [32] to the 730 by 57 binary response matrix, with one primary factor representing the global cognitive ability and five secondary factors. This yields a 57 by 6 factor loading matrix, visualized in Figure 1, where rows correspond to pCAT-COG items and columns represent distinct factors.

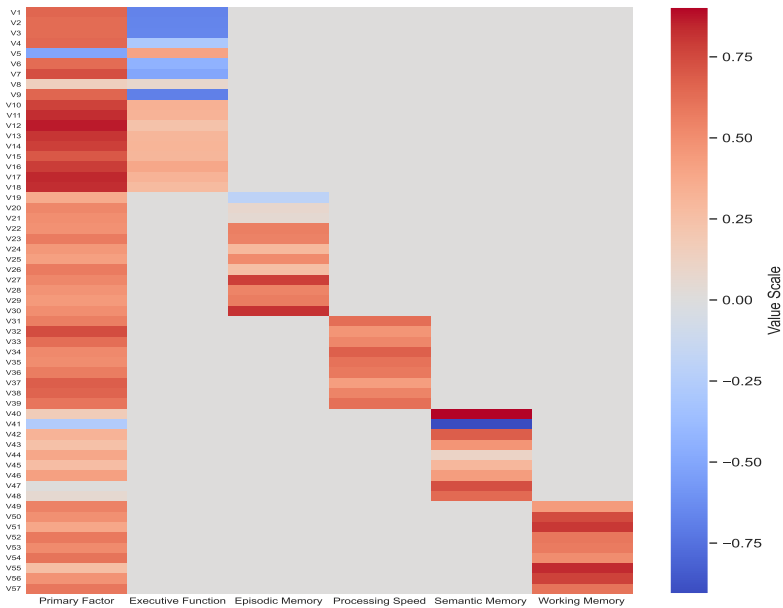


Figure 1: Estimated Bifactor Factor Loading Matrix for pCAT-COG

Our goal is to develop an optimal item selection strategy that efficiently estimates the primary cognitive factor (first column) using the fewest items while maintaining accuracy amid the subdomain influences. Additionally, the selection algorithm must be computationally efficient to navigate a six-dimensional latent space in real time for seamless interactive testing. Online item selection is critical, as learning an optimal sequence from 57 items offline presents an intractable combinatorial problem, even in a binary response setting.

Adaptive cognitive assessment is essential for cognitive assessment, as designing items is costly and administering all items is time-consuming. In Section 6.2, experiments show our deep CAT system terminates testing after an average of 11.1 items, significantly reducing testing burden, minimizing practice effects, and optimizing item bank utilization. The item bank is currently expanding to 500 items with a more nationally representative sample. Success on this prototype dataset paves the way for broader deployment in clinical research.

### 3 From One-Step Optimization to Policy Learning

We formally define the problem of designing a CAT system from a reinforcement learning (RL) perspective. Typical CAT systems consist of two components:

- **Offline Calibration:** An MIRT model is fitted to a calibrated dataset  $Y \in \mathbb{R}^{N \times J}$  to estimate the item characteristic parameters, where  $N$  represents the number of examinees, and  $J$  represents the number of items in the item bank.
- **Online Deployment:** Given the estimated item parameters, an item selection algorithm is deployed online to adaptively select items for future examinees.

The performance of CAT is measured by the number of items required to estimate an examinee’s latent traits with sufficient precision.

### 3.1 Notations and Problem Setups

For the entirety of the paper, we assume the calibration dataset  $Y$  is binary, where each element  $y_{ij}$  represents whether subject  $i$  answered item  $j$  correctly. We consider a general two-parameter MIRT framework with  $K$  latent factors [4]. Let  $B \in \mathbb{R}^{J \times K}$  denote the factor loading matrix, and  $D \in \mathbb{R}^J$  denote the intercept vector. For each examinee  $i$  with multivariate latent trait  $\theta_i \in \mathbb{R}^K$ , the data-generating process for  $y_{ij}$  is given by:

$$y_{ij} | \theta_i, B_j, d_j \sim \text{Bernoulli}(\Phi(B_j' \theta_i + D_j)), \quad (1)$$

where  $B_j$  is the  $j$ -th row of  $B$ ,  $D_j$  is the  $j$ -th entry of  $D$ ,  $\Phi(\cdot)$  represents a standard normal cumulative distribution link function. The item parameters can be compactly expressed as  $\{\xi_j\}_{j=1}^J := \{(B_j, D_j)\}_{j=1}^J$ . This two-parameter MIRT framework is highly general, imposing no structural constraints on the loading matrix and requiring no specific estimation algorithms for item parameter calibration.

Given the estimated item parameters, we need to design an item selection algorithm that efficiently tests a future examinee with unobserved latent ability  $\theta \in \mathbb{R}^K$ . The sequential nature of the CAT problem, combined with recent advancements in Bayesian MIRT [1], makes Bayesian approaches particularly appealing. Without loss of generality, we assume a standard multivariate Gaussian prior on  $\theta \sim N(0, \mathbb{I}_K)$ , and define the following notations:

- For any positive integer  $n$ , let  $[n]$  denote all the positive integers no greater than  $n$ . Let  $j \in [J]$  be the index for the items in the item bank.
- Let  $j_t$  denote the index of the item selected at step  $t$  based on an arbitrary item selection rule. Define  $\mathcal{I}_t$  as the set of the first  $t$  administered items, and let  $R_t := [J] \setminus \mathcal{I}_{t-1}$ , the set of available items before the  $t$ -th item is picked.
- We use the shorthand notation  $f(\theta|Y_{1:T})$  to represent the latent factor posterior distributions  $f(\theta|Y_{1:T}, \xi_{1:T})$  after  $T$  items have been selected. Here, the response history is denoted by  $Y_{1:T} := [y_{j_1}, \dots, y_{j_T}]'$ , and the item parameters are given by  $\xi_{1:T} := (B_{1:T}, D_{1:T})$ , where  $B_{1:T} := [B_{j_1}, \dots, B_{j_T}]'$  and  $D_{1:T} := [D_{j_1}, \dots, D_{j_T}]'$ .

At time  $(t+1)$ , the selection algorithm takes the current posterior  $f(\theta|Y_{1:t})$  as input and outputs the next item selection  $j_{t+1}$ . This process continues until at time  $T'$ , either when the posterior variance of  $f(\theta|Y_{1:T'})$  falls below a predefined threshold  $\tau^2$ , or when  $T' = H$ , where  $H \leq J$  is the maximum number of items that can be administered. Hence the goal of CATs is to minimize  $T'$  given the estimated item parameters of the item bank.

## 3.2 Reviews of Existing Item Selection Rules

Existing item selection rules predominantly rely on one-step-lookahead optimization of some heuristic information-theoretic criteria. For example, the D-optimality criterion [8] selects the next items by maximizing the determinant of the Fisher information matrix. Another approach entails maximizing Kullback-Leibler (KL) information within a Bayesian framework. Recent studies [6, 33] highlight the theoretical and empirical advantages of Bayesian mutual information (MI) over experimental design criteria like D-optimality. These findings underscore the advantages of deploying Bayesian CAT algorithms to enhance estimation accuracy and testing efficiency.

Given that our proposed deep CAT system builds on recent advances in Bayesian MIRT [1], we now review Bayesian item selection rules in greater detail. The popular KL Expected

A Priori (EAP) rule selects the  $t$ -th item based on the average KL distance between response distributions on the candidate item at the EAP estimate  $\hat{\theta}_{t-1} = \int_{\theta} \theta f(\theta|Y_{1:(t-1)})d\theta$ , and random factor  $\theta$  sampled from the posterior distribution  $f(\theta|Y_{1:(t-1)})$  [10]:

$$\arg \max_{j_t \in R_t} \int_{\theta} \left\{ \sum_{l=0}^1 P(y_{j_t} = l|\hat{\theta}_{t-1}) \log \frac{P(y_{j_t} = l|\hat{\theta}_{t-1})}{P(y_{j_t} = l|\theta)} \right\} f(\theta|Y_{1:(t-1)})d\theta \quad (2)$$

Rather than focusing on the KL distance based on the response distributions, the authors in [6] propose the MAX Pos approach by maximizing the KL distance between two subsequent latent factor posteriors  $f(\theta|Y_{1:(t-1)})$  and  $f(\theta|Y_t)$ . Intuitively, this approach prioritizes items that induce the largest shift in the posterior, formalized as:

$$\arg \max_{j_t \in R_t} \sum_{y_{j_t}=0}^1 f(y_{j_t}|Y_{1:(t-1)}) \int_{\theta} f(\theta|Y_{1:(t-1)}) \log \frac{f(\theta|Y_{1:(t-1)})}{f(\theta|Y_{1:t})} d\theta, \quad (3)$$

where  $f(y_{j_t}|Y_{1:(t-1)})$  represents the posterior predictive probability:

$$f(y_{j_t}|Y_{1:(t-1)}) = \int_{\theta} f(y_{j_t}|\theta)f(\theta|Y_{1:(t-1)})d\theta. \quad (4)$$

A third Bayesian strategy, the mutual information (MI) approach, maximizes the mutual information between the current posterior distribution and the response distribution of new item  $y_{j_t}$  [5]. Rooted in experimental design theory [34], we can also interpret mutual information as the entropy reduction of the current posterior estimation of  $\theta$  after observing new response  $y_{j_t}$ . More formally:

$$\arg \max_{j_t \in R_t} I_M(\theta, y_{j_t}) = \arg \max_{j_t \in R_t} \sum_{y_{j_t}=0}^1 \int_{\theta} f(\theta, y_{j_t}|Y_{1:(t-1)}) \log \frac{f(\theta, y_{j_t}|Y_{1:(t-1)})}{f(\theta|Y_{1:(t-1)})f(y_{j_t}|Y_{1:(t-1)})} d\theta. \quad (5)$$

Given the impressive empirical success for the MI method [33], we propose a new heuristic item selection rule that selects items with the highest predictive variance based on the current posterior estimates. Formally, write  $c_{j_t} := f(y_{j_t}|Y_{1:(t-1)})$  as defined in (4), and

consider the following criterion:

$$\operatorname{argmax}_{j_t \in R_t} \int_{\theta} (\Phi(B'_{j_t} \theta + d_{j_t}) - c_{j_t})^2 f(\theta | Y_{1:(t-1)}) d\theta. \quad (6)$$

This rule selects the item  $j_t$  that maximizes the variance of the predictive means, weighted by the current posterior  $f(\theta | Y_{1:(t-1)})$ . Selecting items where examinee’s responses are highly uncertain is advantageous, as administering items with predictable outcomes may lead to inefficient test adaptation. In Appendix A, we establish a connection between this selection rule and the MI method, showing that both favor items with high prediction uncertainty.

### 3.3 Reinforcement Learning Formulation

Existing item selection rules face several limitations: first, these methods rely on one-step-lookahead selection, choosing items that provide the most immediate information without considering their impact on future selections, which can result in suboptimal policies [13]. Second, they are heuristically designed to balance information across all latent factors, rather than emphasizing the most essential factors of interest. In the pCAT-COG study, the goal is to accurately measure the global cognition factor, rather than estimating all latent factors with equal precision. Finally, these rules do not directly minimize test length, potentially increasing test duration without proportional gains in accuracy.

A more principled approach is to formulate item selection as a reinforcement learning (RL) problem, where the optimal policy is learned using Bellman optimality principles rather than relying on heuristics that ignore long-term planning. Beyond addressing myopia, an RL-based formulation can provide a direct mechanism to minimize the number of items required to reach a predefined posterior variance reduction threshold, explicitly guide item selection toward accurately measuring the primary factors of interests.

More generally, consider a general finite horizon setting where each examinee can answer at most  $H \leq J$  items, and the CAT algorithm terminates whenever the posterior variance

of all factors of the interests is smaller than a certain threshold  $\tau^2$ , or when  $H$  is reached. Since  $H$  can be set sufficiently large, it serves as a practical secondary stopping criterion to prevent excessively long tests, and simplifies the policy learning problem. Formally:

- **State Space  $\mathcal{S}$** : the space of all possible latent factor posteriors  $\mathcal{S} := \{f(\theta|Y_{1:t}) : t \in \{1, \dots, H\}\}$ . We may write  $s_t := f(\theta|Y_{1:t})$ , with  $s_0 := N(0, \mathbb{I}_k)$ . The state space is discrete and can be exponentially large. Since there are  $J$  items in the item bank and the responses are binary, the total number of possible states is  $\sum_{t=1}^H \binom{J}{t} \cdot 2^t$ .
- **Action space  $\mathcal{A}$** : the item bank  $[J] := \{1, \dots, J\}$ . However, at the  $t$ -th selection time, the action space is  $R_t := [J] \setminus \mathcal{I}_{t-1}$ , as we do not select the same item twice.
- **Transition Kernel  $\mathcal{P}$**  :  $\mathcal{S} \times \mathcal{A} \rightarrow \Delta(\mathcal{S})$ , where  $\Delta(\mathcal{S})$  is the state of probability distribution over  $\mathcal{S}$ . Conditional on any give state action pair  $(s_t, a_t)$ ,  $s_{t+1}$  can only have two distinct outcomes, depending on whether  $a$  is answered correctly or not.
- **Reward Function**: To directly minimize the test length, we assign a simple 0 – 1 reward structure. In a  $K$ -factor MIRT model, we often prioritize a subset of factors  $\mathcal{K} \subset [K]$  (e.g.  $\mathcal{K} = \{1\}$  for pCAT-COG), with the test terminating once the posterior variances of all factors in  $\mathcal{K}$  fall below the predefined threshold  $\tau^2$ :

$$R^{(t)}(s_t, a, s_{t+1}) = \begin{cases} -1 & \text{if } V_{t+1} > \tau^2, \\ 0 & \text{otherwise,} \end{cases}$$

where  $V_{t+1} = \max_{k \in \mathcal{K}} \text{Var}(\theta_k|Y_t)$  is the maximum marginal posterior variance among the prioritized factors  $\mathcal{K}$ . This also simplifies the learning of the value function, as the rewards are always bounded integers within  $[-H, -1]$ . A similar reward has been successfully deployed in adaptive learning settings [21].

Rather than following a heuristic rule, we consider learning a policy  $\pi(s)$ , defined as a mapping from the current posterior distribution  $s_t$ , to a probabilities of selecting each

remaining item in  $R_t$ . Given a prior distribution  $s_0$ , the value function under  $\pi(s)$  is

$$v_\pi(s_0) := \mathbb{E}_\pi \left[ \sum_{t=0}^{H-1} \gamma^t R^{(t)}(s_t, \pi(s_t), s_{t+1}) | S_0 = s_0 \right], \quad (7)$$

where  $\gamma \in [0, 1)$  is the discount factor. Our goal is to find an optimal policy  $\pi^*(s)$  which maximizes the value function  $v_{\pi^*}(s_0) := \operatorname{argmax}_\pi v_\pi(s_0)$ . To facilitate the search, it is helpful to define the action-value Q function under an arbitrary policy  $\pi(s)$ :

$$Q_\pi(s_0, a) := \mathbb{E}_\pi \left[ \sum_{t=0}^{H-1} \gamma^t R^{(t)}(s_t, \pi(s_t), s_{t+1}) | S_0 = s_0, A_0 = a \right], \quad (8)$$

where action (item)  $a$  is chosen initially. Since  $v_{\pi^*}(s_t) = \max_{a \in R_{t+1}} Q_{\pi^*}(s_t, a)$ , finding  $\pi^*$  amounts to solving the Bellman Equation [18]:

$$Q_\pi(s_t, a_t) = \mathbb{E}_\pi [R(s_t, \pi(s_t), s_{t+1})] + \gamma \sum_{s_{t+1} \in \mathcal{S}} \mathcal{P}(s_{t+1} | s_t, a_t) \max_{a_{t+1} \in \mathcal{R}_{t+2}} Q(s', a'). \quad (9)$$

Since the state space grows exponentially and the transition probabilities unknown, solving for  $\pi^*$  using traditional dynamic programming approaches like value iteration or tabular Q-learning become intractable [13]. In section 5, we propose a double deep Q-learning approach [14, 15] to approximate the optimal policy  $\pi^*(\cdot)$ .

## 4 Accelerating Item Selection via Direct Sampling

Our proposed deep CAT system builds on recent advances in Bayesian MIRT [1], which eliminates rigid constraints on the factor loading matrix and makes our approach highly adaptable across diverse item banks and application domains. By adopting a probit link function, the posterior updates for the multivariate latent factors remain tractable under the MIRT model in Equation (1), thereby bypassing the need for computationally expensive MCMC procedures. This substantial computational improvement not only enhances the efficiency of our proposed Q-learning framework, but also accelerates existing CAT systems.

A key observation is that by repeatedly applying the E-step of the PXL-EM algorithm as introduced in [1], we show that the latent factor posterior distributions belong to an instance of the unified skew-normal distribution [35], defined as follows:

**Definition 4.1.** Let  $\Phi_T \{V; \Sigma\}$  represent the cumulative distribution functions of a  $T$ -dimensional multivariate Gaussian distribution  $N_T(0_T, \Sigma)$  evaluated at vector  $V$ . A  $K$ -dimensional random vector  $\theta \sim \text{SUN}_{K,T}(\xi, \Omega, \Delta, \gamma, \Gamma)$  has the **unified skew-normal distribution** if it has the probability density function:

$$\phi_K(\theta - \xi; \Omega) \frac{\Phi_T \{ \gamma + \Delta' \bar{\Omega}^{-1} \omega^{-1} (\theta - \xi); \Gamma - \Delta' \bar{\Omega}^{-1} \Delta \}}{\Phi_T(\gamma; \Gamma)}.$$

Here,  $\phi_K(\theta - \xi; \Omega)$  is the density of a  $K$ -dimensional multivariate Gaussian with expectation  $\xi = (\xi_1, \dots, \xi_K)'$ , and a  $K$  by  $K$  covariance matrix  $\Omega = \omega \bar{\Omega} \omega$ , where  $\bar{\Omega}$  is the correlation matrix and  $\omega$  is a diagonal matrix with the square roots of the diagonal elements of  $\Omega$  in its diagonal.  $\Delta$  is a  $K$  by  $T$  matrix that determines the skewness of the distribution, and  $\gamma \in \mathbb{R}^T$  control the flexibility in departures from normality.

In addition, the  $(K + T) \times (K + T)$  matrix  $\Omega^*$ , having blocks  $\Omega_{[11]}^* = \Gamma, \Omega_{[22]}^* = \bar{\Omega}$  and  $\Omega_{[21]}^* = \Omega_{[12]}^{*\prime} = \Delta$ , needs to be a full-rank correlation matrix.

Suppose an arbitrary CAT item selection algorithm has already selected  $T$  items with item parameters  $\xi_{1:T} = (B_{1:T}, D_{1:T})$ , where  $B_{1:T} := [B_{j_1}, \dots, B_{j_T}]'$  and  $D_{1:T} := [D_{j_1}, \dots, D_{j_t}]'$ .

Then it is possible to show the following result:

**Theorem 4.2.** Consider a  $K$ -factor CAT item selection procedure after selecting  $T$  items, with  $N(0, \mathbb{I}_K)$  prior placed on the test taker's latent trait  $\theta$ . If  $Y_{1:T} = (y_{j_1}, \dots, y_{j_T})'$  is conditionally independent binary response data from the two-parameter probit MIRT model defined in (1), then

$$(\theta \mid Y_{1:T}, B_{1:T}, D_{1:T}) \sim \text{SUN}_{K,T}(\xi_{\text{post}}, \Omega_{\text{post}}, \Delta_{\text{post}}, \gamma_{\text{post}}, \Gamma_{\text{post}}),$$

with posterior parameters

$$\begin{aligned}\xi_{\text{post}} &= 0_K, & \Omega_{\text{post}} &= \mathbb{I}_K, & \Delta_{\text{post}} &= D_1' D_3^{-1}, \\ \gamma_{\text{post}} &= D_3^{-1} D_2, & \Gamma_{\text{post}} &= D_3^{-1} (D_1 D_1' + \mathbb{I}_T) D_3^{-1},\end{aligned}$$

where  $D_1 = \text{diag}(2y_{j_1} - 1, \dots, 2y_{j_T} - 1) B_{1:T}$  and  $D_2 = \text{diag}(2y_{j_1} - 1, \dots, 2y_{j_T} - 1) D_{1:T}$ . The matrix  $D_3$  is a  $T$  by  $T$  diagonal matrix, where the  $(t, t)$ -th entry is  $(\|B_{t,T}\|_2^2 + 1)^{\frac{1}{2}}$ , with  $B_{t,T}$  representing the  $t$ -th row of  $B_{1:T}$ .

As demonstrated in [35], the distribution of an arbitrary unified skew normal distribution  $\theta \sim \text{SUN}_{K,T}(\xi, \Omega, \Delta, \gamma, \Gamma)$  has a stochastic representation as a linear combination of a  $K$ -dimensional multivariate normal random variable  $V_0$ , and a  $T$ -dimensional truncated multivariate normal random variable  $V_{1,-\gamma}$  as follows:

$$\theta \stackrel{d}{=} \xi + \omega(V_0 + \Delta \Gamma^{-1} V_{1,-\gamma}), \quad (10)$$

where  $V_0 \sim N(0, \bar{\Omega} - \Delta \Gamma^{-1} \Delta') \in \mathbb{R}^K$  and  $V_{1,-\gamma}$  is obtained by component-wise truncation below  $-\gamma$  of a variate  $N(0, \Gamma) \in \mathbb{R}^T$ .

Based on Theorem 4.2 and equation (10), sampling from latent factor posterior distribution  $f(\theta|Y_{1:T})$  requires two independent steps: sampling from a  $K$ -dimensional multivariate normal distribution, and a  $T$ -dimensional multivariate truncated normal distribution. As a result, the direct sampling approach scales efficiently with the number of factors  $K$ , since generating samples from  $K$ -dimensional multivariate normal distributions is trivial. Moreover, in CAT settings, the test is typically terminated early, meaning  $T$  remains relatively small. When  $T$  is moderate (e.g,  $T < 1,000$ ), sampling from the truncated multivariate normal distribution remains computationally efficient using the minimax tilting method of Botev [17]. The exact proof of Theorem 4.2 and the sampling details can be found in Appendix B.1 and B.2 respectively.

Theorem 4.2 plays a central role in our proposed deep Q-learning algorithm, as it fully characterizes the latent factor posterior distribution  $f(\theta|Y_{1:T})$ , enabling parametrization of the state variable  $s_T$ , which serves as an input to the Q-network illustrated in Section 5.1. Furthermore in Section 4.1, we demonstrate how our method improves the efficiency of common Bayesian item selection rules, while in Section 4.2, we extend our approach to fully Bayesian online computation, incorporating uncertainty in the item parameters.

## 4.1 Accelerating Existing Rules

A major contribution of this work is the acceleration of all existing Bayesian item selection rules discussed in Section 3.2. For example, in computing the KL-EAP item selection rule (2), we directly sample from  $f(\theta|Y_{1:(t-1)})$  instead of resorting to MCMC, and evaluate the integral via Monte-Carlo integration. Since the EAP estimate  $\hat{\theta}_{t-1}$  remains fixed at time step  $t$ , evaluating the KL information term straightforward.

To compute the Max Pos item selection rule in equation (3), we obtain i.i.d. samples from  $f(\theta|Y_{1:(t-1)})$  and compute the posterior predictive probabilities in (4) via Monte-Carlo integration. Although the density ratio  $\frac{f(\theta|Y_{1:(t-1)})}{f(\theta|Y_{1:t})}$  is extremely difficult to evaluate, we can leverage the conditional independence assumption of the MIRT model. Suppose  $(t-1)$  items have already been selected, and recall  $y_{jt}$  represents the binary response for item  $j_t$ , should it be selected at time  $t$ . Then we can express the joint distribution of  $(\theta, y_{jt})$  as

$$f(\theta, y_{jt}|Y_{1:(t-1)}) = f(\theta|Y_{1:(t-1)}, y_{jt})f(y_{jt}|Y_{1:(t-1)}) = f(y_{jt}|\theta)f(\theta|Y_{1:(t-1)}). \quad (11)$$

Using Equation (11), we rewrite the KL information term in Equation (3) as:

$$\begin{aligned} \int f(\theta|Y_{1:(t-1)}) \log \frac{f(\theta|Y_{1:(t-1)})}{f(\theta|Y_{1:(t-1)}, y_{jt})} d\theta &= \int f(\theta|Y_{1:(t-1)}) \log \frac{f(\theta|Y_{1:(t-1)})f(y_{jt}|Y_{1:(t-1)})}{f(\theta, Y_{jt}|Y_{1:(t-1)})} d\theta \\ &= \int f(\theta|Y_{1:(t-1)}) \log \frac{f(y_{jt}|Y_{1:(t-1)})}{f(y_{jt}|\theta)} d\theta. \end{aligned}$$

Since  $f(y_{j_t}|Y_{1:(t-1)})$  has already been computed, and  $f(y_{j_t}|\theta)$  can be easily computed for each  $\theta \sim f(\theta|Y_{1:(t-1)})$ , the online-computation of Mas Pos remains efficient.

Although the mutual information selection rule in Equation (5) has demonstrated strong empirical performance [33], its computational complexity remains a significant challenge. By applying Equation (11), we can rewrite mutual information as

$$\arg \max_{j_t \in R_t} \sum_{y_{j_t}=0}^1 f(y_{j_t}|Y_{1:(t-1)}) \int_{\theta} f(\theta|Y_{1:(t-1)}, y_{j_t}) \log \frac{f(y_{j_t}|\theta)}{f(y_{j_t}|Y_{1:(t-1)})} d\theta. \quad (12)$$

This formulation reveals that maximizing mutual information is structurally similar to Max Pos but requires much more computational efforts. Unlike Max Pos, where sampling is performed from the current posterior  $f(\theta|Y_{1:(t-1)})$ , mutual information requires sampling from future posteriors  $f(\theta|Y_{1:(t-1)}, y_{j_t})$ . Since each candidate item  $j_t \in R_t$  has two possible outcomes ( $y_{j_t} = 0$  or  $y_{j_t} = 1$ ), evaluating equation (12) requires obtaining samples from  $|R_t| \times 2$  distinct posterior distributions. Even if sampling each individual posterior is computationally efficient, this approach becomes impractical for large item banks.

We hence propose a new approach to dramatically accelerate the computation of the mutual information quantity using the idea of importance sampling and resampling and bootstrap filter [36, 37]. Rather than explicitly sampling the future posterior  $f(\theta|Y_{1:(t-1)}, y_{j_t})$  for each  $j_t \in R_t$  and  $y_{j_t} \in \{0, 1\}$ , we can simply sample from the current posterior  $f(\theta|Y_{1:(t-1)})$  once, and then perform proper posterior reweighing. Under equation (1), let  $p(\theta)$  be the prior on the latent factors  $\theta$ ,  $l_1(\theta)$  be the current data likelihood, and  $l_2(\theta)$  denote the future data likelihood after observing  $y_{j_t}$ . We have the future posterior density as below:

$$\begin{aligned} f(\theta|Y_{1:(t-1)}, y_{j_t}) &\propto l_2(\theta)p(\theta) \propto \frac{l_2(\theta)p(\theta)}{l_1(\theta)p(\theta)} f(\theta|Y_{1:(t-1)}) \\ &= \Phi(B'_{j_t}\theta + d_{j_t})^{y_{j_t}} (1 - \Phi(B'_{j_t}\theta + d_{j_t}))^{1-y_{j_t}} f(\theta|Y_{1:(t-1)}). \end{aligned} \quad (13)$$

Equation (13) suggests we can generate samples from  $f(\theta|Y_{1:(t-1)}, y_{j_t})$  via reweighting and resampling from the current posterior samples  $f(\theta|Y_{1:(t-1)})$ . Specifically, given a sufficient large set of posterior samples  $(\theta_1, \dots, \theta_M) \sim f(\theta|Y_{1:(t-1)})$ , we assign distinct weights for each sample  $m \in [M]$  and future item  $j_t \in R_t$ :

$$q_m = \frac{w_m}{\sum_{i=1}^M w_i}, \quad \text{where } w_i = \Phi(B'_{j_t} \theta_i + d_{j_t})^{y_{j_t}} (1 - \Phi(B'_{j_t} \theta_i + d_{j_t}))^{1-y_{j_t}}.$$

To sample from  $f(\theta|Y_{1:(t-1)}, y_{j_t})$ , we then draw from the discrete distribution over  $(\theta_1, \dots, \theta_M)$ , placing weight  $q_m$  on  $\theta_m$ . This approach eliminates the need to sample from  $|R_t| \times 2$  distinct posteriors directly, further accelerating mutual information computation and making it scalable for large item banks.

## 4.2 Fully Bayesian Item Selections

Another key advantage of our direct sampling approach is its ability to enable fully Bayesian item selection. Since Section 3, we have assumed that the item bank is well-calibrated, allowing the factor loading matrix and the intercept to be treated as fixed. This assumption is only reasonable when large calibration datasets are available, as item parameters can be reliably estimated from the data. While this is a prevailing assumption in the literature, it is important to acknowledge that it can lead to overly optimistic estimates of the uncertainties in the multidimensional latent traits.

A fully Bayesian framework offers a principled way to incorporate this uncertainty by integrating over the joint posterior of item parameters and latent traits. However, performing this integration in online item selection has long been considered intractable, limiting its practical adoption. Notably, [38] introduced an efficient MCMC method, but only for unidimensional item response theory model.

Our direct sampling approach extends fully Bayesian item selection to multivariate IRT while avoiding the computational bottlenecks of MCMC. To illustrate, we consider the

mutual information criterion in (12). Fully Bayesian inference involves obtaining posterior samples of item parameters  $\{\xi^{(m)}\}_{m=1}^M$ , where  $\xi^{(m)} := (B^{(m)}, D^{(m)})$ . The mutual information criterion in Equation (12) requires computing the posterior predictive probability:

$$f(y_{jt}|Y_{1:(t-1)}) = \int_{\xi} \int_{\theta} f(y_{jt}|\theta) f(\theta|\xi, Y_{1:(t-1)}) d\theta d\xi. \quad (14)$$

Similarly, the KL divergence term must integrate out nuisance item parameters  $\xi$ :

$$\int_{\xi} \int_{\theta} f(\theta|Y_{1:(t-1)}, y_{jt}, \xi) \log \frac{f(y_{jt}|\theta)}{f(y_{jt}|Y_{1:(t-1)})} d\theta d\xi. \quad (15)$$

By leveraging Theorem 4.2, we can exactly identify the posterior distributions for any arbitrary configuration of  $f(\theta|Y_{1:(t-1)}, y_{jt}, \xi^{(m)})$ , hence enabling direct sampling in parallel. It follows Equations (14) and (15) are computationally feasible via Monte Carlo integration.

In contrast, a standard MCMC approach requires constructing  $M$  independent Markov chains, each targeting  $f(\theta|Y_{1:(t-1)}, y_{jt}, \xi^{(m)})$ , with sampling only possible after all chains have reached convergence. This introduces a significant computational burden, making MCMC impractical for real-time item selection. Although our primary focus is not on fully Bayesian item selection, we demonstrate the computational efficiency of our direct sampling approach in Appendix C through a nontrivial three-factor, 150-item simulation.

## 5 Learning Optimal Item Selection Policy

In Section 3.3, we highlight the necessity of transforming the one-step-lookahead optimization of heuristic information-theoretic criteria into a more principled RL-based item selection policy. An RL approach addresses the myopic nature of these selection rules, enables a more flexible reward structure, and directly minimizes the number of items required for performing online adaptive testing. Learning the optimal item selection policy requires solving the Bellman equation in Equation (9). Since the transition kernel  $\mathcal{P}$  is unknown

and the state space exponentially large, a natural solution is to use a deep neural network to approximate the optimal action-value function  $Q^*(s, a)$ .

We hence propose a novel double Q-learning algorithm [14, 15] for online item selection in CAT. The algorithm trains a deep neural network offline using item parameters estimated from an arbitrary two-parameter MIRT model. During online item selection, the neural network takes the current posterior distribution  $s_t := f(\theta | Y_{1:t})$  as input and outputs the next item selection for step  $(t + 1)$ . The neural network architecture is described in Section 5.1, while the double deep Q-learning algorithm is detailed in Section 5.2.

## 5.1 Deep Q-learning Neural Network Design

A potential reason why a deep reinforcement learning approach has not been proposed in the CAT literature is due to the ambiguity arising from unidentified latent factor distributions. However, by Theorem 4.2, it is straightforward to compactly parametrize the posterior distribution  $s_t := f(\theta|Y_{1:t})$  at each time step  $t$  using the parameters  $D_1 \in \mathbb{R}^{t \times K}$ ,  $D_2 \in \mathbb{R}^t$ , and  $\text{diag}(D_3) \in \mathbb{R}^t$ , where  $\text{diag}(D_3)$  represents the diagonal vector of  $D_3$ . Rather than feeding the entire response history and item parameters to the neural network, this structured and compact representation eliminates the ambiguity in posterior updates, facilitating the integration of deep reinforcement learning into CAT frameworks.

Define the collection of the posterior parameters  $\tilde{\xi}_t := \{(D_{1h}, D_{2h}, D_{3h})\}_{h=1}^t$ , where  $D_{1h}$  is the  $h$ -th row of  $D_1$ ,  $D_{2h}$  is the  $h$ -th element of  $D_2$ , and  $D_{3h}$  is the  $h$ -th elements in the diagonal of  $D_3$ . Since the size of the posterior parameters  $\tilde{\xi}_t$  grows over time, and permuting the tuples within  $\tilde{\xi}_t$  still describes the same posterior, we have to design a neural network that can take inputs of growing size, and can provide output that is permutation invariant of the inputs. One solution is to consider the weight sharing idea appeared in the Bayesian experimental design literature [25]: Let  $\phi_1$  denote the feature mapping applied for each tuple in  $\tilde{\xi}_t$ , and we define the encoder  $g_1$  as follows:

$$g_1(\tilde{\xi}_t) := \sum_{h=1}^t \phi_1\{(D_{1h}, D_{2h}, D_{3h})\}. \quad (16)$$

Observe the encoder  $g_1(\cdot)$  is capable of handling growing number of inputs, and will produce the same output regardless of the order of the tuples appeared in  $\tilde{\xi}_t$ . Although the form of  $g_1$  may look restrictive, any function  $f(\cdot)$  operating on a countable set can be decomposed into the form  $\rho \circ g_1(\cdot)$ , where  $\rho(\cdot)$  is a suitable transformation that can be learned from another neural network (see Theorem 2 of [39]).

In principle, the network design  $\rho \circ g_1(\cdot)$ , coupled with the Q-learning algorithm is sufficient to learn the optimal policy, and can be deployed offline with significantly less computational cost since it does not require either sampling or optimization. However, to enhance learning efficiency, we advocate for augmenting the current input space  $\tilde{\xi}_t$  with a matrix of prediction quartiles  $\Psi_t \in \mathbb{R}^{J \times Q}$ , where each row contains a vector of quantiles of the predictive mean distribution for item  $j$ . These distributions can be formed by drawing samples  $\theta_1, \dots, \theta_M \sim f(\theta|Y_{1:t})$  as described in Section 4, and then computing the quantiles of the prediction samples  $\{\Phi(B'_j \theta_i + d_j)\}_{i=1}^M$  for each item  $j$ . Since sampling from  $f(\theta|Y_{1:t})$  only needs to be done once, computing the matrix  $\Psi_t$  online is computationally efficient.

The motivation for augmenting the input space with  $\Psi_t$  is to provide the neural network with additional contextual information in addition to the current posterior parameters. By incorporating the full predictive distribution through  $\Psi_t$ , the neural network has the capacity to extract more nuanced patterns, potentially leading to faster convergence to the optimal item selection policies. Additionally,  $\Psi_t$  also serves to discourage the network from selecting previously administered items, as their prediction uncertainties are minimal.

In summary, to select the  $(t+1)$ -th item, our proposed neural net takes two inputs: the posterior parameters  $\tilde{\xi}_t$  and the prediction matrix  $\Psi_t$ , and outputs the selected item. Let  $\phi_2$  represent the component processing the matrix  $\Psi_t \in \mathbb{R}^{J \times Q}$ , and  $\phi_3$  the hidden layers that maps the concatenated feature spaces from  $g_1(\cdot)$  and  $\phi_2$  to a  $J$ -dimensional logits

vector. Denoting the final policy network as  $\pi_\phi$ , our proposed network selects the item corresponding the maximum value of the following softmax function:

$$\pi_\phi(\tilde{\xi}_t, \Psi_t) := \text{Softmax} \left\{ \phi_3 \{g_1(\tilde{\xi}_t), \phi_2(\Psi_t)\} \right\}.$$

## 5.2 Double Deep Q-Learning for CAT

The standard Q-learning algorithm often overestimates Q-values because the Q-network selects actions based on maximization operations, which are then used in network evaluation during training. To address this issue, we adopt the Double Q-learning approach [15], which uses a primary network to select the best action and a separate target network to evaluate it. This separation results in more accurate Q-value approximations and leads to a more stable training process.

Our proposed algorithm is presented in Algorithm table 1. Note that for the Q-learning to converge to an optimal policy, it is essential to adopt an  $\epsilon$ -greedy policy, where the algorithm makes random item selections with probability  $\epsilon$  and gradually decreases  $\epsilon$  over the course of training. For simplicity, the state variable  $s_t$  in Algorithm 1 is a compact representation of  $(\tilde{\xi}_t, \Psi_t)$  defined in Section 5.1. In practice, we can terminate the training process when both the rewards and the validation loss stabilize, indicating that the neural network has well approximated the optimal policy.

## 5.3 Remark on the Choice of Reward Functions

The simple 0-1 reward structure offers several advantages. It is interpretable as it directly minimizes the number of items required to terminate cognitive assessment tasks and prioritizes the main factors of interest. Additionally, it has demonstrated effectiveness in related problems, such as deep adaptive learning [21]. Since the cumulative reward is constrained to integer values between  $-H$  and  $-1$ , the action-value function can be more reliably approximated by the neural network, thus stabilizing the training process.

---

**Algorithm 1:** Double Q-Learning Algorithm for Bayesian CAT

---

**Input** : Total Episodes  $E$ ,  $\epsilon \in [\underline{\epsilon}, \bar{\epsilon}]$  with  $\epsilon^{(0)} = \bar{\epsilon}$ , buffer  $\mathcal{H}$ , target network update frequency  $T$ , batch size  $M$ .

**Output** : Learned Q-network  $Q^A$  for item selection.

**Model parameters:** Primary Q-network  $Q^A$ , target Q-network  $Q^B$ .

Initialize primary Q-network  $Q^A$  and target Q-network  $Q^B$ , with weights  $w_0^A = w_0^B$ ;

**for**  $i = 1$  **to**  $E$  **do**

- Draw  $\theta_i$  from  $N(0, I_k)$ ;
- Set initial state  $s_0 := N(0, I_k)$  and available item set  $R_0 = \{1, \dots, J\}$ ;
- for**  $t = 0$  **to**  $H$  **do**
  - Select action  $a_t$  using  $\epsilon$ -greedy policy:
$$a_t = \begin{cases} \text{Random Selection} & \text{with probability } \epsilon^{(t)} \\ \arg \max_{a \in R_t} \hat{Q}^A(s_t, a) & \text{otherwise.} \end{cases}$$
  - Observe response  $y_t$ ;
  - Update available item set  $R_{t+1} = R_t \setminus a_t$ ;
  - Obtain new state  $s_{t+1}$  and compute reward  $r_t$ ;
  - if**  $r_t = 0$  **then**
    - | Break and proceed to the next episode;
  - end**
  - Store transition  $H_{i,t} := (s_t, a_t, r_t, R_t, s_{t+1})$  into buffer  $\mathcal{H}$ ;
  - if**  $|\mathcal{H}| > \text{batch size } M$  **then**
    - | Randomly sample  $M$  transitions  $\{H_{i,t}\}_{j=1}^M$  from  $\mathcal{H}$ ;
    - | Compute  $a_j = \arg \max_{a \in R_j} \hat{Q}^A(s_t, a)$ ;
    - | Compute target:
$$y^{(j)} = \begin{cases} -1 & r_j = 0 \\ -1 + \gamma \hat{Q}^B(s'_j, a_j) & \text{otherwise.} \end{cases}$$
    - | Perform batch gradient descent on loss:  $\sum_{j=1}^M (y^{(j)} - \hat{Q}^A(s_j, a_j))^2$ ;
  - end**
  - Decrease  $\epsilon^{(t)}$  if  $\epsilon^{(t)} \geq \underline{\epsilon}$ ;
- end**
- Update target network  $Q^B$  such that  $w_t^A = w_t^B$  if  $i$  is a multiple of  $T$ ;

**end**

---

While our double Q-learning algorithm can accommodate alternative reward functions to our proposed 0-1 reward, its advantages over greedy one-step-lookahead policy may be limited for certain reward structures. In [40], it is shown that for stochastic depletion problems, a myopic policy achieves at least 50% of the expected reward of the optimal

policy. A similar result can be proven for CAT under specific reward structures. To illustrate this, we extend the state space  $\mathcal{S}$  with a time variable, defining  $\bar{\mathcal{S}} = \{(f(\theta | Y_{1:t}), t) : t \in [H]\}$ . Let  $\pi^*(\bar{s})$  represent the optimal policy, and  $\pi^m(\bar{s})$  the myopic policy that maximizes the next-step expected reward. Define the mapping  $\hat{G}_{y_a} : \bar{s} \rightarrow \bar{s}'$  as the posterior update after observing the binary response random variable  $y_a$ , with an incremented time step, where  $\bar{s} = (f(\theta|Y_{1:t}), t)$  and  $\bar{s}' = (f(\theta|Y_{1:t}, y_a), t + 1)$ . Similarly, define  $\tilde{G}_{y_a} : \bar{s} \rightarrow \bar{s}'$  as the posterior update after observing  $y_a$  while keeping the time step fixed, where  $\bar{s} = (f(\theta|Y_{1:t}), t)$  and  $\bar{s}' = (f(\theta|Y_{1:t}, y_a), t)$ .

To demonstrate the near-optimality of the myopic policy, [40] introduces two key assumptions: “value function monotonicity” and “immediate rewards”. These assumptions can be adapted to the CAT setting as follows:

- **Immediate Rewards:** for any time stamp  $t < H$ , suppose the myopic policy  $\pi^m$  chooses item  $a$ , then we must have

$$V_{\pi^*}(\bar{s}) \leq E[R(\bar{s}, a, \bar{s}')] + V_{\pi^*}(\tilde{G}_{y_a}(\bar{s})). \quad (17)$$

Essentially, the property says given a free item (without increasing the time step) chosen by the myopic policy would not deteriorate the optimal rewards.

- **Value Function Monotonicity:** for any time stamp  $t < H$ , suppose the optimal policy would choose item  $a_1$  yet the myopic policy would chooses item  $a_2$ , then

$$V_{\pi^*}(\hat{G}_{y_{a_2}}(\tilde{G}_{y_{a_1}}(\bar{s}))) \leq V_{\pi^*}(\hat{G}_{y_{a_2}}(\bar{s})). \quad (18)$$

Note both sides of inequality refer to the optimal value function evaluated at the posterior distribution at time step  $t + 1$ .

In Theorem 5.1, we establish that a reinforcement learning approach to CAT cannot significantly outperform the one-step-lookahead greedy policy when the reward function satisfies

the two assumptions outlined above. The proof is provided in Appendix D.

**Theorem 5.1.** *Consider the finite horizon CAT problem with  $H$  steps. Suppose the assumptions of immediate rewards in (17) and value function monotonicity in (18) hold, we have  $V_{\pi^*}(\bar{s}) \leq 2V_{\pi^m}(\bar{s})$  for all  $\bar{s} \in \bar{\mathcal{S}}$ .*

Theorem 5.1 can be seen as a limitation of the reinforcement learning approach when the reward structure aligns with the stochastic depletion problem, as it implies that a simple myopic policy provides a 2-approximation to the optimal policy. However, it also highlights the advantage of the simple 0-1 reward function as the value function monotonicity is unlikely to hold, rendering the theorem inapplicable. Specifically, the expected posterior variance of  $\hat{G}_{y_{a_2}}(\tilde{G}_{y_{a_1}}(\bar{s}))$  is expected to be smaller than that of  $\hat{G}_{y_{a_2}}(\bar{s})$ . Consequently, fewer items are expected for the posterior  $\hat{G}_{y_{a_2}}(\tilde{G}_{y_{a_1}}(\bar{s}))$  to reach the minimum variance threshold, which implies  $V_{\pi^*}(\hat{G}_{y_{a_2}}(\tilde{G}_{y_{a_1}}(\bar{s}))) \geq V_{\pi^*}(\hat{G}_{y_{a_2}}(\bar{s}))$ .

In contrast, if we set the reward as maximizing the cumulative variance reduction over  $H$  steps, the value function monotonicity assumption is more likely to hold. This is because cumulative variance reduction starting from a posterior with smaller variance is expected to be less than that from a posterior with larger variance, given the same remaining item budgets. We may also expect the immediate reward property to hold, as the right hand side of equation (17) has an additional item in the budget, and the expected variance reduction is nonnegative. Thus, Theorem 5.1 provides valuable guidance in avoiding reward structures where the reinforcement learning approach may offer limited advantages.

## 6 Experiments

To comprehensively evaluate the effectiveness of our proposed deep CAT system against other item selection benchmarks, we define the *oracle posterior distribution* of a test taker as the posterior obtained if this test taker had answered all items in the item bank. This represents the best Bayesian estimates achievable given the available item bank.

## 6.1 Simulations

We randomly generated a 5-factor, 200-item factor loading matrix  $B \in \mathbb{R}^{200 \times 5}$ . The matrix was initially constructed by assigning each column a random permutation of 200 equally spaced values, with loading magnitude bounded by  $[0.3, 0.9]$ , ensuring diverse loadings while restricting the slope magnitude by 3. To better reflect real-world datasets, where items rarely load on all five factors, each item was allowed to load on at most two factors. Additionally, the intercepts for each item were uniformly sampled from  $(-1.5, 1.5)$ .

To evaluate our approach in a more challenging setting, we extend the estimation target to the first three factors ( $\mathcal{K} = \{1, 2, 3\}$ ), while accounting for the presence of factors 4 and 5. Leveraging our proposed direct sampling approach outlined in Section 4, we implemented our double Q-learning algorithm alongside all existing methods discussed in Section 3.2. These include the EAP approach (Equation 2), the Max Pos approach (Equation 3), the MI approach (Equation 5), and the Max Var approach (Equation 6).

For the Q-learning algorithm, we trained the Q-network for 40,000 episodes, with exploration parameter  $\epsilon$  decreasing linearly from 0.99 to 0.01 over 750,000 steps. We set a sufficient large  $H = 70$  items, with discount factor  $\gamma = 0.95$ . To make sure the double Q-learning algorithm indeed converges to the optimal policy  $\pi^*$ , we provide further details on the training dynamics of our deep Q-learning algorithm, illustrating the increase in rewards and the decrease in validation loss until convergence in Appendix E.1.

To evaluate termination efficiency, we start with the standard multivariate Gaussian prior  $\theta \sim N(0, \mathbb{I}_5)$  and dynamically terminate the test once the maximum posterior variance across *all three* target factors in  $\mathcal{K}$  falls below  $\tau^2 < 0.16$ . Based on 500 simulated adaptive testing sessions, Figure 2 illustrates how the percentage of completed test sessions increases as more items are administered. Faster growth rate of the completion percentages indicates faster posterior variance reduction. Notably, the purple Q-learning curve consistently grows above all curves, demonstrating significant testing efficiency gains. As summarized in the

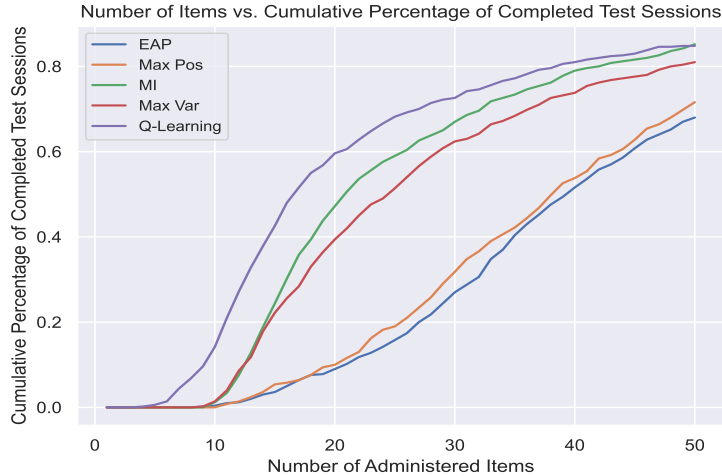


Figure 2: Number of Items Versus Cumulative Percentage of Completed Tests

Table 1: Comparison of Winshares (W.S), Termination, and Computation

Algorithm	Avg Termination (items)	W.S dim0	W.S dim1	W.S dim2	Avg Time (s/item)
EAP	37.6	17.6%	14.8%	11.6%	<b>0.025</b>
Max Pos	36.6	15.2%	13.4%	12.4%	0.028
MI	25.8	21.6%	20.2%	25.0%	0.084
Max Var	27.7	<b>23.0%</b>	24.4%	23.0%	0.036
Q-learning	<b>22.4</b>	22.6%	<b>27.2%</b>	<b>28.0%</b>	0.067

second column of Table 1, Q-learning requires an average of only 22.4 items to reach the termination criterion for all 3 targeted factors, outperforming all other methods.

Figure 3 illustrates how the mean squared error (MSE) between the posterior mean and the oracle posterior mean decreases as more items are administered. The MSE for each latent dimension is averaged over 500 simulated adaptive sessions. Consistent with variance reduction, Q-learning achieves excellent MSE reduction rate. To quantify this, we compute the MSEs after 20 items for each test sessions and determine win shares, defined as the percentage of test takers for whom each method achieves the lowest MSE after 20 items. These win shares are reported across all three latent dimensions in Table 1. Notably, Q-learning achieves the lowest MSE in dimensions 1 and 2, while slightly trailing Max Var in dimension 0. Furthermore, Q-learning provides better approximations of the full oracle distributions, extending beyond the posterior mean, as detailed in Appendix E.2.

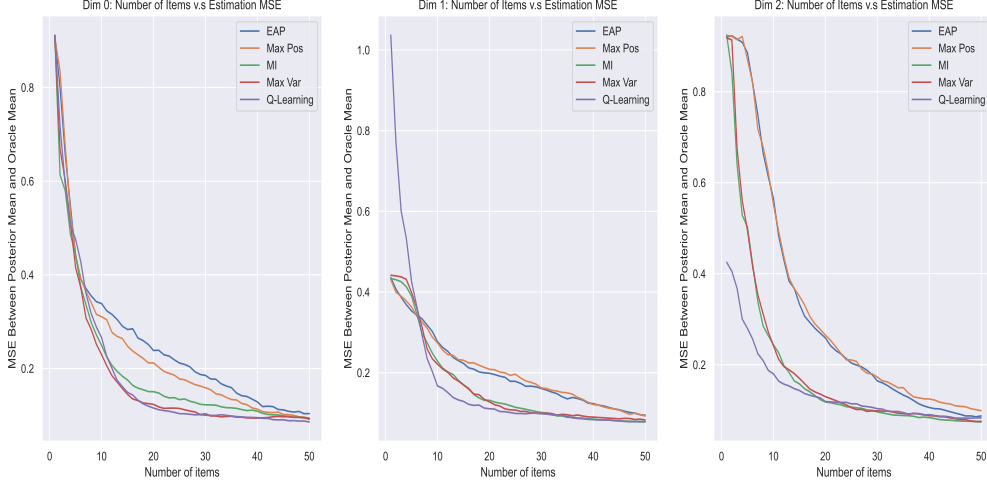


Figure 3: MSE Between Posterior Means and Oracle Posterior Means

The last column of Table 1 reports the average item selection time, highlighting the significant computational advantages of our direct sampling approach. Even the most computationally intensive MI approach requires only 0.084 seconds per item selection, via our proposed posterior reweighting strategy. While Q-learning involves computation of the feed-forward Q-network, it remains relatively fast. Although we trained the Q-network using a single GPU, we emphasize that the online Q-learning item selection time was computed without GPU acceleration, demonstrating its accessibility on standard laptops.

## 6.2 Cognitive Function Measurements

We revisit the problem of designing a deep CAT system for the pCAT-COG study, as outlined in Section 2. Since item response data for all  $N = 730$  examinees across  $J = 57$  items is available, we can directly use real item responses during evaluation rather than simulating testing sessions. Furthermore, by Theorem 4.2, we can efficiently compute the oracle posteriors for each examinee, which provide a more realistic basis for evaluating the estimation accuracy of our proposed CAT framework.

Given that pCAT-COG is designed to measure global cognitive ability (first column

in Figure 1) while accounting for five cognitive subdomains, we specified the Q-learning reward function to reduce posterior variance for the primary factor ( $\mathcal{K} = \{1\}$ ). This demonstrates the flexibility of our CAT system, as it can be tailored to the specific cognitive assessment needs. While the existing policies in Section 3.2 possess desirable information-theoretic properties, adapting them to prioritize the most clinically relevant dimension proved challenging. This is particularly evident in the bifactor model, where every item loads on the primary dimension with lack of independence, complicating item selection.

The left subplot of Figure 4 shows that Q-learning again achieves the fastest test termination compared to other methods. As before, the test is dynamically terminated when the posterior variance drops below  $\tau^2 = 0.16$ , and the cumulative percentage of completed test sessions is computed over all 730 examinees. The first row of Table 2 shows that Q-learning reaches the desired posterior variance reduction threshold after only an average of 11.1 items. All item selection algorithms terminated earlier than the previous simulation study, which required the posterior variance for all three factors to fall below  $\tau^2$ .

Beyond fast variance reduction, the right subplot of Figure 4 highlights the rapid decay of mean squared error (MSE) in estimating the primary dimension with Q-learning. For further comparison, we consider adaptively selecting 20 items for each test taker without dynamic termination. We chose the number 20 because the Max Pos approach required the largest average of 19.8 items for termination. The second row of Table 2 shows that the Q-learning approach achieves the highest 0.958 correlation between the estimated primary factor posterior means and the oracle ones after only 20 items. Additionally, Q-learning approach attains the highest win shares in estimating the primary dimension across all  $N = 730$  examinees. Although Q-learning did not outperform all methods across all subdomains, these subdomains are not of direct clinical interests.

This experiment highlights the effectiveness of our Q-learning approach in high-dimensional cognitive function measurement. Unlike approaches that learn a fixed test design offline

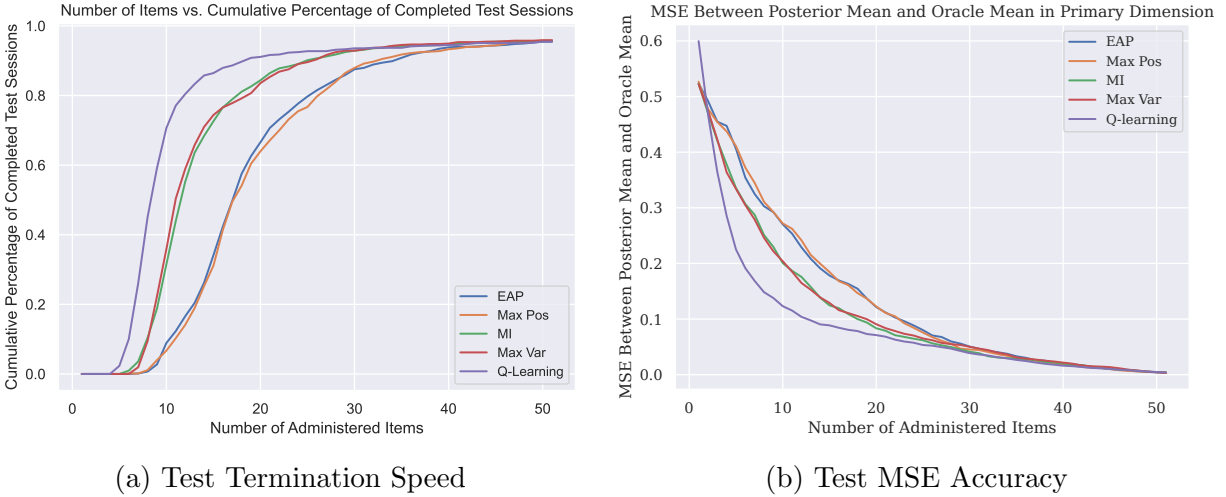


Figure 4: pCAT-COG: Primary Factor Posterior Variance Reduction (Left) and Estimation Accuracy (Right)

Table 2: Comparison of Winshares (W.S), Termination, and Computation

Metric	EAP	Max Pos	MI	Max Var	Q-Learning
<b>Avg Termination (items)</b>	19.5	19.8	14.4	14.2	<b>11.1</b>
<b>Primary Factor Correlation</b>	0.920	0.918	0.950	0.948	<b>0.958</b>
<b>W.S Primary Factor</b>	15.9%	15.9%	17.6%	20.7%	<b>29.9%</b>
<b>W.S Executive Function</b>	16.8%	17.1%	21.2%	19.6%	<b>25.3%</b>
<b>W.S Episodic Memory</b>	12.6%	14.9%	22.6%	<b>31.4%</b>	18.5%
<b>W.S Processing Speed</b>	15.2%	16.4%	20.7%	22.7%	<b>25.0%</b>
<b>W.S Semantic Memory</b>	11.4%	8.9%	<b>36.2%</b>	32.5%	11.0%
<b>W.S Working Memory</b>	17.0%	16.2%	20.5%	<b>23.3%</b>	23.0%
<b>Avg Time (s/item)</b>	<b>0.018</b>	0.019	0.028	0.020	0.031

[41], our framework enables fully dynamic item selection, maximizing the utilization of the item bank by exploring diverse testing trajectories. This termination efficiency is particularly valuable in cognitive assessment, where item development is costly, and can help mitigate practice effects and preserves items for future use.

### 6.3 Educational Assessments

We consider an important application in educational assessment, utilizing 2022 Grade 8 student item response data from the Massachusetts Department of Elementary and Secondary Education (DESE). Excluding non-multiple-choice questions, the dataset includes

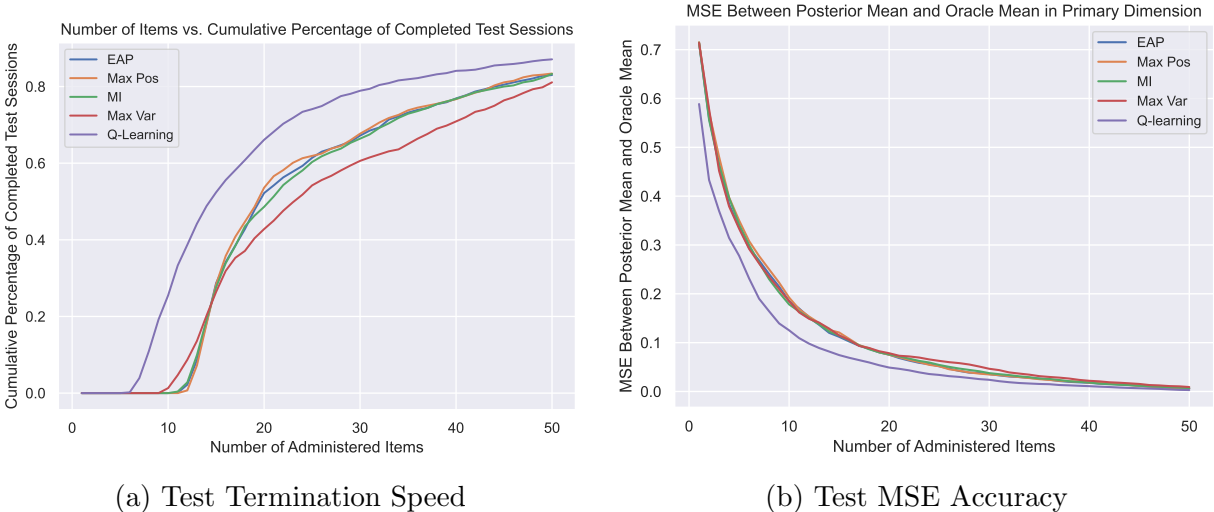


Figure 5: Educational Assessment: Main Factor Posterior Variance Reduction (Left) and Estimation Accuracy (Right)

responses to 24 English items and 34 math items. For efficiency, we randomly sampled 1,000 student responses to evaluate each CAT item selection algorithm.

Given the unknown latent structure, we estimate the factor loading matrix via the PXL-EM algorithm [1], resulting in a 58 by 4 factor loading matrix, with visualization and the details of model fitting provided in Appendix F. Since all items are heavily loaded on the first primary factor, representing the global latent ability, we focus on the problem of adaptively measuring the first factor while accounting for the underlying multidimensional structure in dimensions 2-4.

The left subplot of Figure 5 illustrates the cumulative percentage of completed test sessions for the 1,000 sampled examinees as more items are administered. As in previous experiments, the Q-learning algorithm exhibits the fastest variance reduction, significantly increasing the test completion rate. On average, Q-learning required only 20 items to reach the termination criterion, whereas the second-fastest method (MI) required nearly 26 items. Beyond its efficiency in variance reduction, Q-learning also achieves a faster decay in MSE when estimating the first factor, reinforcing findings from earlier experiments.

These results highlight the potential of Q-learning for educational assessments, demon-

strating its ability to adapt various testing environments and to accelerate testing while maintaining accurate estimation of students’ multivariate latent traits.

## 7 Discussion

This work advocates for a deep reinforcement learning perspective in the design of multidimensional computerized adaptive testing systems. We make two key contributions to the existing CAT literature: (1) a computational advancement that accelerates online item selection within a flexible Bayesian MIRT framework [1], and (2) a novel reinforcement learning-based approach that mitigates myopic decision-making and prioritizes the assessment of primary factors of interest.

Theorem 4.2 not only provides an efficient parameterization of the latent factor posterior distributions for our proposed deep Q-learning approach, but also improves existing CAT item selection algorithms, as detailed in Section 4. Leveraging direct sampling from unified skew-normal distributions, our methodology scales efficiently with a large number of factors and items, achieving near-instantaneous online selection by circumventing MCMC sampling, while imposing no strict factor loading constraints on the item bank. Additionally, our approach naturally extends to fully Bayesian item selection by accounting for uncertainties in item parameters, which is an essential consideration when the item bank is not well-calibrated. Throughout the testing trajectory, our approach precisely characterizes the evolution of posterior distributions at each time step, providing a more robust measurement process beyond point estimates with difficult-to-compute standard errors.

Another key contribution of this work is the development of a robust deep double Q-learning algorithm with a customized reward structure that directly minimizes test length. As demonstrated in both simulations and real-data studies, our Q-learning algorithm consistently achieves the fastest posterior variance reduction while rapidly decreasing estimation bias. Moreover, its flexible reward function allows adaptation to different testing objec-

tives, providing a principled framework for designing customized tests and overcoming the myopic nature of traditional CAT methods.

Our work also offers practical guidance for selecting the appropriate item selection algorithms. Unlike the existing heuristic rules, our deep CAT system requires offline Q-network training before deployment. For the pCAT-COG study, training took approximately one day on a single GPU, but no GPU is needed for fast online item selection. Even when offline training is impractical, our framework significantly accelerates existing methods. Experiments show that MI (Equation 5) and our maximizing variance (Equation 6) approaches often outperform other heuristic rules, providing a strong alternative to Q-learning.

A promising direction for future work is to extend our methods to more general data types, such as ordinal and categorical datasets. Recent work [1] shows that the latent factor posterior distribution under mixed binary and ordinal data retains the form of unified skew-normal distribution. While this structure allows for efficient approximation, direct sampling from it remains challenging, potentially hindering rapid online selection. Developing more effective sampling schemes will be crucial to accommodating these broader data types.

Another exciting avenue is to explore alternative reward structures for our Q-learning algorithm. While the 0-1 reward structure is interpretable and stabilizes Q-network training, it provides sparse feedback, which may limit empirical performance. Alternative designs could incorporate intermediate rewards or increased penalization as more items are administered. An interesting theoretical direction is to characterize when reinforcement learning approaches are particularly advantageous compared to myopic methods. This requires careful assumptions about the reward function and the item bank’s properties, providing deeper insights into the trade-offs between RL and traditional item selection strategies.

## References

- [1] Jiguang Li, Robert Gibbons, and Veronika Rockova. Sparse bayesian multidimensional item response theory. *Journal of the American Statistical Association*, 2025.

- [2] Wim J. van der Linden and Cees A. W. Glas. *Elements of Adaptive Testing*. Springer, New York, 2010.
- [3] Robert D. Gibbons, David J. Weiss, Ellen Frank, and David Kupfer. Computerized adaptive diagnosis and testing of mental health disorders. *Annual Review of Clinical Psychology*, 12:83–104, 2016. Epub 2015 Nov 20.
- [4] R.D. Bock and R.D. Gibbons. *Item Response Theory*. Wiley, 2021.
- [5] Alexander Weissman. Mutual information item selection in adaptive classification testing. *Educational and Psychological Measurement*, 67(1):41–58, 2007.
- [6] Joris Mulder and Wim Linden. *Multidimensional Adaptive Testing with Kullback–Leibler Information Item Selection*, pages 77–101. 01 2010.
- [7] Robert Gibbons, Diane Lauderdale, Robert Wilson, David Bennett, Tesnim Arar, and David Gallo. Adaptive measurement of cognitive function based on multidimensional item response theory. *Alzheimer’s & Dementia: Translational Research & Clinical Interventions*, 10, 11 2024.
- [8] Daniel O. Segall. Multidimensional adaptive testing. *Psychometrika*, 61(2):331–354, 1996.
- [9] Wim J. van der Linden. Multidimensional adaptive testing with a minimum error-variance criterion. *Journal of Educational and Behavioral Statistics*. Forthcoming, year unknown.
- [10] Bernard Veldkamp and Wim Linden. Multidimensional adaptive testing with constraints on test content. *Psychometrika*, 67(4):575–588, December 2002.
- [11] Hua-Hua Chang. Psychometrics behind computerized adaptive testing. *Psychometrika*, 80(1):1–20, March 2015.
- [12] Hua-Hua Chang and Zhiliang Ying. a-stratified multistage computerized adaptive testing. *Applied Psychological Measurement*, 23(3):211–222, 1999.
- [13] Richard S. Sutton and Andrew G. Barto. *Reinforcement Learning: An Introduction*. The MIT Press, second edition, 2018.
- [14] Volodymyr Mnih, Koray Kavukcuoglu, David Silver, Andrei A. Rusu, Joel Veness, Marc G. Bellemare, Alex Graves, Martin Riedmiller, Andreas K. Fidjeland, Georg Ostrovski, Stig Petersen, Charles Beattie, Amir Sadik, Ioannis Antonoglou, Helen King, Dhharshan Kumaran, Daan Wierstra, Shane Legg, and Demis Hassabis. Human-level control through deep reinforcement learning. *Nature*, 518:529–533, 2015.
- [15] Hado van Hasselt, Arthur Guez, and David Silver. Deep reinforcement learning with double q-learning. *Proceedings of the AAAI Conference on Artificial Intelligence*, 30(1), Mar. 2016.

- [16] Daniele Durante. Conjugate bayes for probit regression via unified skew-normal distributions. *Biometrika*, 106(4):765–779, aug 2019.
- [17] Z. I. Botev. The normal law under linear restrictions: Simulation and estimation via minimax tilting. *Journal of the Royal Statistical Society Series B: Statistical Methodology*, 79(1):125–148, feb 2016.
- [18] Dimitri P. Bertsekas and John N. Tsitsiklis. *Neuro-Dynamic Programming*. Athena Scientific, 1st edition, 1996.
- [19] David Silver, Aja Huang, Chris J. Maddison, Arthur Guez, Laurent Sifre, George Van Den Driessche, Julian Schrittwieser, Ioannis Antonoglou, Veda Panneershelvam, Marc Lanctot, Sander Dieleman, Dominik Grewe, John Nham, Nal Kalchbrenner, Ilya Sutskever, Timothy Lillicrap, Madeleine Leach, Koray Kavukcuoglu, Thore Graepel, and Demis Hassabis. Mastering the game of go with deep neural networks and tree search. *Nature*, 529(7587):484–489, 2016.
- [20] Dmitry Kalashnikov, Alex Irpan, Peter Pastor, Julian Ibarz, Alexander Herzog, Eric Jang, Deirdre Quillen, Ethan Holly, Mrinal Kalakrishnan, Vincent Vanhoucke, and Sergey Levine. Qt-opt: Scalable deep reinforcement learning for vision-based robotic manipulation. *ArXiv*, abs/1806.10293, 2018.
- [21] Xiao Li, Hanchen Xu, Jinming Zhang, and Hua hua Chang. Deep reinforcement learning for adaptive learning systems. *Journal of Educational and Behavioral Statistics*, 48(2):220–243, 2023.
- [22] Tom Rainforth, Adam Foster, Desi R. Ivanova, and Freddie Bickford Smith. Modern Bayesian Experimental Design. *Statistical Science*, 39(1):100 – 114, 2024.
- [23] Kathryn Chaloner and Isabella Verdinelli. Bayesian Experimental Design: A Review. *Statistical Science*, 10(3):273 – 304, 1995.
- [24] Paola Sebastiani and Henry P. Wynn. Maximum entropy sampling and optimal bayesian experimental design. *Journal of the Royal Statistical Society. Series B (Statistical Methodology)*, 62(1):145–157, 2000.
- [25] Adam Foster, Desi R. Ivanova, Ilyas Malik, and Tom Rainforth. Deep adaptive design: Amortizing sequential bayesian experimental design. In *International Conference on Machine Learning*, 2021.
- [26] Donald R Jones, Matthias Schonlau, and William J Welch. Efficient global optimization of expensive black-box functions. *Journal of Global Optimization*, 13(4):455–492, 1998.
- [27] Niranjana Srinivas, Andreas Krause, Sham M Kakade, and Matthias W Seeger. Gaussian process optimization in the bandit setting: No regret and experimental design. In *Proceedings of the 27th International Conference on Machine Learning (ICML)*, pages 1015–1022. Omnipress, 2010.

- [28] Philipp Hennig and Christian J. Schuler. Entropy search for information-efficient global optimization. *Journal of Machine Learning Research*, 13:1809–1837, 2012.
- [29] Remi Lam, Karen Willcox, and David H. Wolpert. Bayesian optimization with a finite budget: An approximate dynamic programming approach. In D. Lee, M. Sugiyama, U. Luxburg, I. Guyon, and R. Garnett, editors, *Advances in Neural Information Processing Systems*, volume 29. Curran Associates, Inc., 2016.
- [30] Alzheimer’s Association. 2024 alzheimer’s disease facts and figures. *Alzheimer’s & Dementia*, 20(5), 2024.
- [31] Alison R. Huang, Kiersten L. Strombotne, Elizabeth Mokyr Horner, and Susan J. Lapham. Adolescent cognitive aptitudes and later-in-life alzheimer disease and related disorders. *JAMA Network Open*, 1(5):e181726–e181726, 09 2018.
- [32] Robert D. Gibbons and Donald Hedeker. Full-information item bi-factor analysis. *Psychometrika*, 57(3):423–436, September 1992.
- [33] Chun Wang and Hua-hua Chang. Item selection in multidimensional computerized adaptive testing—gaining information from different angles. *Psychometrika*, 76(3):363–384, 07 2011. Copyright - The Psychometric Society 2011; Last updated - 2023-12-03.
- [34] Alfréd Rényi. On measures of entropy and information. 1961.
- [35] Reinaldo B. Arellano-Valle and Adelchi Azzalini. On the unification of families of skew-normal distributions. *Scandinavian Journal of Statistics*, 33(3):561–574, 2006.
- [36] Neil J. Gordon, David Salmond, and Adrian F. M. Smith. Novel approach to nonlinear/non-gaussian bayesian state estimation. 1993.
- [37] A. F. M. Smith and A. E. Gelfand. Bayesian statistics without tears: A sampling-resampling perspective. *The American Statistician*, 46(2):84–88, 1992.
- [38] Wim J. van der Linden and Hao Ren. A fast and simple algorithm for bayesian adaptive testing. *Journal of Educational and Behavioral Statistics*, 45(1):58–85, 2020.
- [39] Manzil Zaheer, Satwik Kottur, Siamak Ravanbakhsh, Barnabás Póczos, Ruslan Salakhutdinov, and Alexander J Smola. Deep sets. In *Proceedings of the 31st International Conference on Neural Information Processing Systems*, NIPS’17, page 3394–3404, Red Hook, NY, USA, 2017. Curran Associates Inc.
- [40] Carri W. Chan and Vivek F. Farias. Stochastic depletion problems: Effective myopic policies for a class of dynamic optimization problems. *Mathematics of Operations Research*, 34(2):333–350, 2009.
- [41] Chelsea Krantsevich, P. Richard Hahn, Yi Zheng, and Charles Katz. Bayesian decision theory for tree-based adaptive screening tests with an application to youth delinquency. *Annals of Applied Statistics*, 17(2):1038–1063, June 2023.

# Supplementary Material: Deep Computerized Adaptive Testing

## A Mutual Information as Prediction Uncertainties

We observe all the heuristic Bayesian item selection methods discussed in this manuscript account for prediction uncertainty. In particular, the mutual information item selection rule can be rewritten as follows:

$$\begin{aligned}
 \arg \max_{j_t \in R_t} I_M(\theta, y_{j_t}) &= \arg \max_{j_t \in R_t} \sum_{y_{j_t}=0}^1 \int_{\theta} f(\theta, y_{j_t} | Y_{t-1}) \log \frac{f(\theta, y_{j_t} | Y_{t-1})}{f(\theta | Y_{t-1}) f(y_{j_t} | Y_{t-1})} d\theta \\
 &= \arg \max_{j_t \in R_t} \sum_{y_{j_t}=0}^1 \int_{\theta} f(y_{j_t} | \theta) f(\theta | Y_{t-1}) \log \frac{f(\theta, y_{j_t} | Y_{t-1})}{f(\theta | Y_{t-1}) f(y_{j_t} | Y_{t-1})} d\theta \\
 &= \arg \max_{j_t \in R_t} \sum_{y_{j_t}=0}^1 \int_{\theta} f(y_{j_t} | \theta) f(\theta | Y_{t-1}) \log \frac{f(y_{j_t} | \theta)}{f(y_{j_t} | Y_{t-1})} d\theta \\
 &= \arg \max_{j_t \in R_t} \int_{\theta} [\Phi(B'_{j_t} \theta + d_{j_t}) \log \frac{\Phi(B'_{j_t} \theta + d_{j_t})}{c_{j_t}} + \\
 &\quad (1 - \Phi(B'_{j_t} \theta + d_{j_t})) \log \frac{(1 - \Phi(B'_{j_t} \theta + d_{j_t}))}{(1 - c_{j_t})}] f(\theta | Y_{t-1}) d\theta. \tag{19}
 \end{aligned}$$

Equation (19) suggests the mutual information criterion selects the item  $j_t$  that has the largest expected KL divergence between the Bernoulli distributions parametrized by  $\Phi(B'_{j_t} \theta + d_{j_t})$  and  $c_{j_t}$ , weighted by the current posterior  $f(\theta | Y_{t-1})$ .

Observe that mutual information essentially favors the item  $j_t$  that has the largest prediction uncertainties around its prediction mean  $c_{j_t}$ , quantified by the KL divergence. To compare equation (19) with equation (6), note we have replace the integral of KL divergence from  $c_{j_t}$  with variances  $(\Phi(B'_{j_t} \theta + d_{j_t}) - c_{j_t})^2$  in (6). This suggests that our proposed approach shares similar theoretical properties with the mutual information criterion, but offers a much simpler formula for online computation, avoiding posterior reweighting and log transformations. Empirically, our proposed item selection rule achieves comparable performance to mutual information but with significantly reduced computational time.

## B Sequential Sampling in CAT

### B.1 Proof of Theorem 4.2

For any  $T \geq 1$ , we may write the likelihood of item response after administering  $T$  items under the two-parameter probit MIRT model as follows:

$$\begin{aligned} \prod_{t=1}^T \Phi(B'_{jt}\theta + d_{jt})^{y_{jt}} (1 - \Phi(B'_{jt}\theta + d_{jt}))^{1-y_{jt}} &= \prod_{t=1}^T \Phi\{(2y_{jt} - 1)(B'_{jt}\theta + d_{jt})\} \\ &= \Phi_T\{((D_1\theta + D_2); \mathbb{I}_T)\}. \end{aligned}$$

Given the standard multivariate normal prior  $\theta \sim N(0, \mathbb{I}_K)$ , the posterior can be expressed as follows:

$$\begin{aligned} \pi(\theta|Y_{1:T}, B_{1:T}, D_{1:T}) &\propto \phi_K(\theta; \mathbb{I}_k) \Phi_T\{((D_1\theta + D_2); \mathbb{I}_T)\} \\ &= \phi_K(\theta; \mathbb{I}_k) \Phi_T\{D_3^{-1}((D_1\theta + D_2); D_3^{-1}D_3^{-1})\} \\ &= \phi_K(\theta; \mathbb{I}_k) \Phi_T\{D_3^{-1}D_2 + D_3^{-1}D_1\theta; D_3^{-1}D_3^{-1}\} \end{aligned}$$

To identify the exact posterior parameters, we draw back to our attention to the probability kernel of the unified skewed-normal distribution as defined in Definition 4.1. It is immediately obvious that

$$\xi_{\text{post}} = 0_K, \quad \Omega_{\text{post}} = \mathbb{I}_K, \quad \text{and} \quad \gamma_{\text{post}} = D_3^{-1}D_2.$$

Recall that  $\Omega = \omega\bar{\Omega}\omega$  as the decompose of covariance matrix into correlation matrix, we have  $\bar{\Omega} = \omega = \mathbb{I}_K$ . It remains to solve the following two linear equation:

$$\begin{aligned} \Delta'\bar{\Omega}^{-1}\omega^{-1} &= D_3^{-1}D_2 \\ \Gamma - \Delta'\bar{\Omega}^{-1}\Delta &= D_3^{-1}D_3^{-1}. \end{aligned}$$

It follows that  $\Delta_{\text{post}} = D_1'D_3^{-1}$  and

$$\Gamma_{\text{post}} = D_3^{-1}D_3^{-1} + D_3^{-1}D_1D_1'D_3^{-1} = D_3^{-1}(D_1'D_1 + \mathbb{I}_T)D_3^{-1}.$$

Finally, to show this is indeed a unified skewed-normal distribution, we need to show  $\Omega^*$  is a full-rank correlation matrix. To see this, we may decompose  $\Omega^*$  as follows:

$$\begin{bmatrix} D_3^{-1}(D_1D_1' + \mathbb{I}_T)D_3^{-1} & D_3^{-1}D_1 \\ D_1'D_3^{-1} & \mathbb{I}_K \end{bmatrix} = \begin{bmatrix} D_3^{-1} & 0 \\ 0 & \mathbb{I}_k \end{bmatrix} \times \begin{bmatrix} D_1D_1' + \mathbb{I}_T & D_1 \\ D_1' & \mathbb{I}_k \end{bmatrix} \times \begin{bmatrix} D_3^{-1} & 0 \\ 0 & \mathbb{I}_k \end{bmatrix}.$$

Observe that this is a decomposition of correlation matrix, where the middle matrix above is the covariance matrix of a  $(T + K)$  dimensional random vector  $[z_1', z_2']'$ , where  $z_1 = D_1z_2 + \epsilon$ ,  $z_2$  is a  $K$ -dimensional standard multivariate Gaussian vector with identity covariance matrix, and  $\epsilon$  is a  $T$ -dimensional standard multivariate Gaussian vector, independent of  $z_2$ .

## B.2 Sequential Sampling Algorithms

For any Bayesian item selection algorithms or our proposed deep CAT framework, it is essential to sample from the latent factor posterior distributions  $f(\theta|Y_{1:t})$  for any  $t \geq 1$ . Theorem 4.2 provides a direct sampling approach to perform such sequential sampling, hence circumventing the need for MCMC algorithms, where cannot be parallelized and required additional tuning and mixing time.

The key observation is that any unified skew-normal distribution  $\theta \sim \text{SUN}_{K,T}(\xi, \Omega, \Delta, \gamma, \Gamma)$  has the stochastic representation as  $\theta \stackrel{d}{=} \xi + \omega(V_0 + \Delta\Gamma^{-1}V_{1,-\gamma})$ , where  $V_0 \sim N(0, \bar{\Omega} - \Delta\Gamma^{-1}\Delta') \in \mathbb{R}^K$  and  $V_{1,-\gamma}$  is obtained by component-wise truncation below  $-\gamma$  of a variate  $N(0, \Gamma) \in \mathbb{R}^T$ . By plugging in the posterior parameters derived in Theorem 4.2, we have the representation

$$\theta \sim V_0 + D_1'(D_1D_1' + \mathbb{I}_t)^{-1}D_3V_{1,-\gamma}.$$

Hence we can conduct efficient sequential posterior sampling using the following three steps when  $t > 1$ :

- **Step One:** Sample from multivariate normal distribution

$$V_0 \sim N(0, \mathbb{I}_K - D_1'(D_1D_1' + \mathbb{I}_T)^{-1}D_1).$$

- **Step two:** Leveraging the minimax tilting method [17], sample from the zero-mean  $T$ -variate truncated multivariate normal distribution  $V_{1,-\gamma}$  with covariance matrix  $D_3^{-1}(D_1D_1' + \mathbb{I}_T)D_3^{-1}$  and truncation below  $-D_3^{-1}D_2$ .
- **Step three:** perform linear computation  $V_0 + D_1'(D_1D_1' + \mathbb{I}_T)^{-1}D_3V_{1,-\gamma}$ .

Table 3: Comparison of Winshares (W.S), Termination, and Computation

Algorithm	Avg Termination (items)	W.S dim0	W.S dim1	W.S dim2	Avg Time (s/item)
EAP	24.4	22.2%	19.2%	21.8%	4.10
Max Pos	24.2	17.4%	18.0%	21.0%	4.10
MI	<b>18.7</b>	<b>32.8%</b>	31.0%	27.8%	4.11
Max Var	19.2	27.6%	<b>31.8%</b>	<b>29.4%</b>	4.10

Note for  $t = 1$ , the sampling steps above can be modified into their univariate analog. Since steps one and step two are independent, one can simply perform i.i.d sampling from both  $V_0$  and  $V_1$  in parallel to draw large samples of  $\theta \sim f(\theta|Y_{1:t})$  in the probit MIRT model. The  $t \times t$  matrix inverse  $(D_1 D_1' + \mathbb{I}_t)$  is easy to compute and only needs to be computed once.

## C Fully Bayesian Item Selection Simulation

We evaluate the effectiveness of our direct sampling approach in enabling fully Bayesian online item selection. Unlike traditional methods that treat item parameters as fixed, the fully Bayesian approach explicitly accounts for their uncertainties, which can be substantial when the item response dataset is small or poorly calibrated. To illustrate, we generate a binary item response dataset  $Y$  with  $N = 500$  examinees and  $J = 150$  items under a 3-factor probit MIRT model. The true factor loading matrix  $B$  has dimensions  $J \times 3$ , and the intercept vector  $D$  has 150 elements.

To integrate item parameter uncertainty into online item selection, we fit a Gibbs sampler to the  $N \times J$  item response data. We generated 5,000 MCMC draws, retaining the last 500 posterior samples of the item parameters  $\Xi = \xi^{(m)}_{m=1}^{500}$  after burn-in. As described in Section 4.2, the fully Bayesian approach marginalizes over the joint distributions of the nuisance item parameters  $\Xi$  and latent traits. We then implemented all item selection rules depicted in Sections 3.2 in a fully Bayesian manner.

Figure 6 illustrates the cumulative percentage of completed test sessions across all 500 simulated examinees as more items are administered. The test was dynamically terminated when the posterior standard deviations across all three factors fell below 0.4. Consistent with the experimental results in Section 6 of the manuscript, the mutual information method and our proposed Max Var method demonstrated superior posterior variance reduction. The second column of Table 3 shows that the mutual information method terminated after an average of 18.7 items, whereas the EAP approach required 24.4 items.

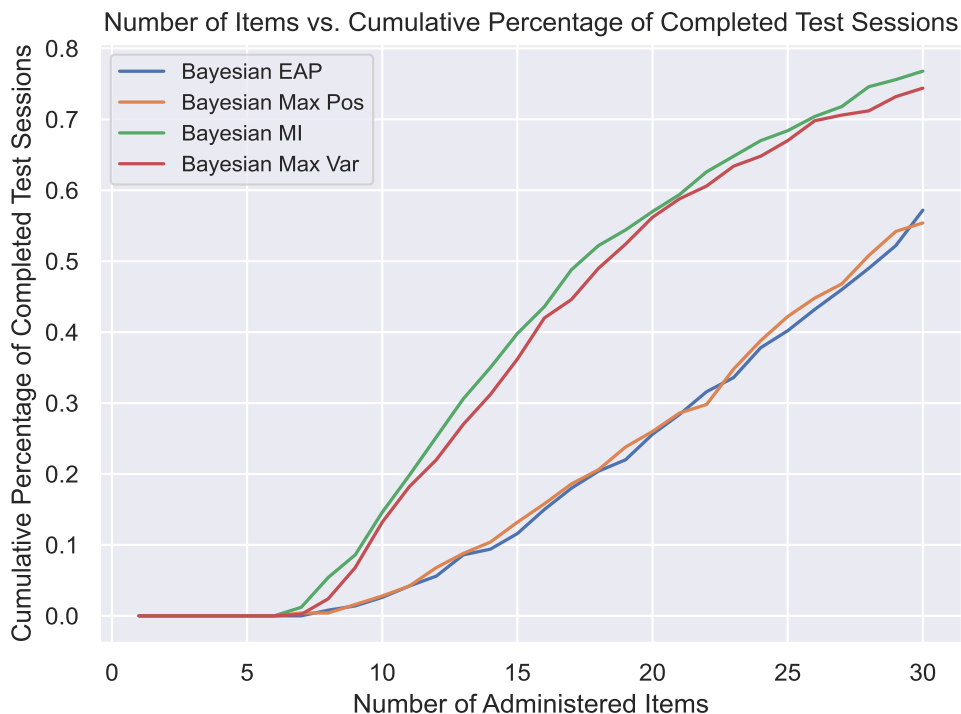


Figure 6: Fully Bayesian: Number of Items Versus Posterior Variance Reduction

Beyond variance reduction, the mutual information and maximizing prediction variance methods also exhibited superior estimation accuracy, as shown in Figure 7, which tracks the decline in mean squared error (MSE) between the posterior mean and the oracle posterior mean. Since estimation errors stabilized around  $H = 30$  items, we compared MSEs between the posterior mean at  $H = 20$  and the oracle posterior mean, and then summarized the win shares for each item selection rule across all 500 examinees and all three dimensions in Table 3.

Finally, we emphasize that even in a fully Bayesian framework, where nuisance parameters are integrated rather than fixed, our approach remains computationally efficient. Across all item selection rules, online selection required an average of just 4.1 seconds per test session on a personal laptop, highlighting the scalability of our direct sampling method for Bayesian MCAT applications. Readers may notice that 4.1 seconds is significantly longer than the item selection time reported in the experimentation section, where item parameters are treated as fixed. This discrepancy arises because fully Bayesian MCAT requires sampling from  $M = 500$  distinct unified-skew normal distributions for each item selection, whereas the standard case involves sampling from a single fixed distribution. This also explains the minimal differences in item selection time across algorithms, as the

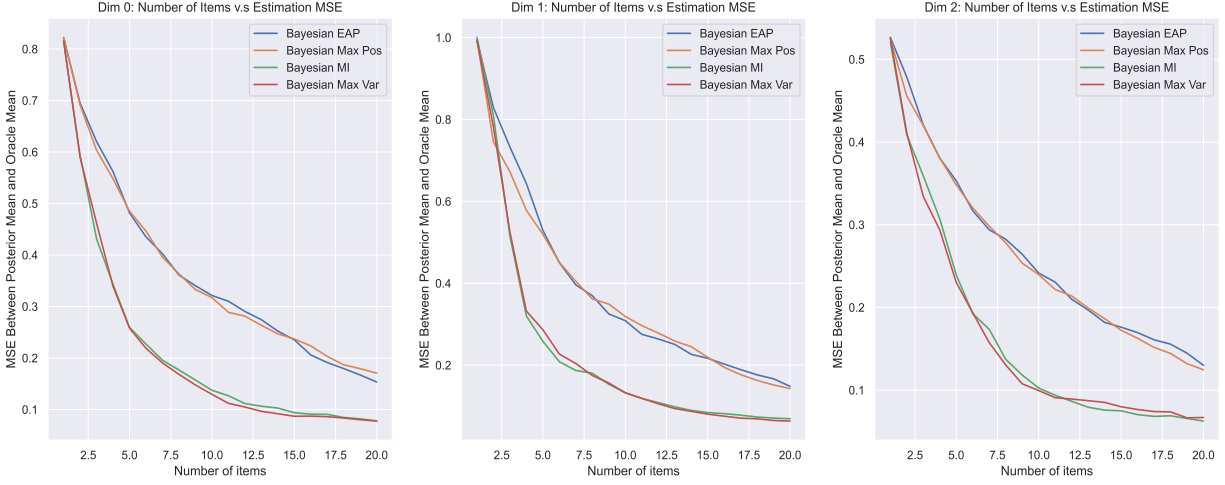


Figure 7: Fully Bayesian: MSE Between Posterior Mean and Oracle Posterior Mean

primary computational bottleneck lies in sampling from these distributions. When more CPUs are available, we can certainly sampling from all  $M$  distributions in parallel, and hence further improving the 4.1 seconds benchmark.

## D Proof of Theorem 5.1

*Proof.* We proceed by induction. Since the myopic and the optimal policy would agree on time  $t = H - 1$ , the inequality holds trivially for the base case. For the induction step, we assume the claimed inequality holds for all  $t'$  such that  $H > t' > t$ . Consider the time horizon  $t < t'$  and let  $a_1$  represent the item chosen by the optimal policy and  $a_2$  the item chosen by the myopic policy. The inequality holds trivially for  $a_1 = a_2$ . Hence, we consider the case when  $a_1 \neq a_2$  and let  $y_{a_1}$  and  $y_{a_2}$  represent the binary random variables for the item response. For given extended state  $\bar{s}$ , we use  $\bar{s}'$  to denote the next step after selecting an item. Then we have

$$\begin{aligned}
 V_{\pi^*}(\bar{s}|y_{a_1}, y_{a_2}) &= E[R(\bar{s}, a_1, \bar{s}')|y_{a_1}] + V_{\pi^*}(\hat{G}_{y_{a_1}}(\bar{s})) \\
 &\leq E[R(\bar{s}, a_1, \bar{s}')|y_{a_1}] + E[R(\bar{s}, a_2, \bar{s}')|y_{a_2}] + V_{\pi^*}(\tilde{G}_{y_{a_2}}(\hat{G}_{y_{a_1}}(\bar{s}))) \quad (20)
 \end{aligned}$$

$$\begin{aligned}
 &= E[R(\bar{s}, a_1, \bar{s}')|y_{a_1}] + E[R(\bar{s}, a_2, \bar{s}')|y_{a_2}] + V_{\pi^*}(\hat{G}_{y_{a_1}}(\tilde{G}_{y_{a_2}}(\bar{s}))) \\
 &\leq E[R(\bar{s}, a_1, \bar{s}')|y_{a_1}] + E[R(\bar{s}, a_2, \bar{s}')|y_{a_2}] + V_{\pi^*}(\hat{G}_{y_{a_2}}(\bar{s})) \quad (21)
 \end{aligned}$$

$$\leq E[R(\bar{s}, a_1, \bar{s}')|y_{a_1}] + E[R(\bar{s}, a_2, \bar{s}')|y_{a_2}] + 2V_{\pi^m}(\hat{G}_{y_{a_2}}(\bar{s})). \quad (22)$$

Note we applied the immediate rewards assumption in equation (20), the value function monotonicity assumption in equation (21), and the induction hypothesis in equation (22). Now, we may take expectation over  $y_{a_1}$  and  $y_{a_2}$  on both side of inequality and obtain:

$$\begin{aligned} V_{\pi^*}(\bar{s}) &\leq E[R(\bar{s}, a_1, \bar{s}')] + E[R(\bar{s}, a_2, \bar{s}')] + 2V_{\pi^m}(\hat{G}_{y_{a_2}}(\bar{s})) \\ &\leq 2(E[R(\bar{s}, a_2, \bar{s}')] + V_{\pi^m}(\hat{G}_{y_{a_2}}(\bar{s}))) = 2V_{\pi^m}(\bar{s}). \end{aligned}$$

The last inequality is due to the fact the  $\pi^m$  is the myopic policy that maximizes the next step reward.  $\square$

## E More Analysis on Simulation

### E.1 Double Q-Learning Training Dynamics

In Figure 8, we present two key metrics illustrating the training dynamics of our Q-learning algorithm. The left subplot displays the average episode rewards, computed over every 500 training episodes, showing that rewards began converging around episode 20,000 at approximately  $-25$ . The right subplot shows the average validation loss, also computed over every 500 episodes, indicating convergence around a loss value of 2. Given that  $H = 70$  in this experiment, the reward is bounded within  $[-70, 1]$ , and the observed MSE of 2 between the primary and target network suggests good convergence.

Since we save the primary neural network every 500 episodes, we select the checkpoint corresponding to the highest average reward for offline deployment in future item selection tasks. In this case, the network at episode 35,000 is chosen, as it achieves the peak average reward of approximately  $-24.4$ . This model selection strategy is consistently applied across all experiments in Section 5.

### E.2 Matching the Oracle Posterior

Recall the "oracle posterior distribution" of a test taker is defined as the posterior obtained if the given test taker had answered all items in the item bank. To obtain the oracle distributions for each of the 500 test taker in Section 6.1, we simulate their item response to all 200 items in the test bank, and then calculate the posterior distribution using Theorem 4.2.

Figures 9, 10, and 11 illustrate the decrease of the estimation MSE for the first quartile,

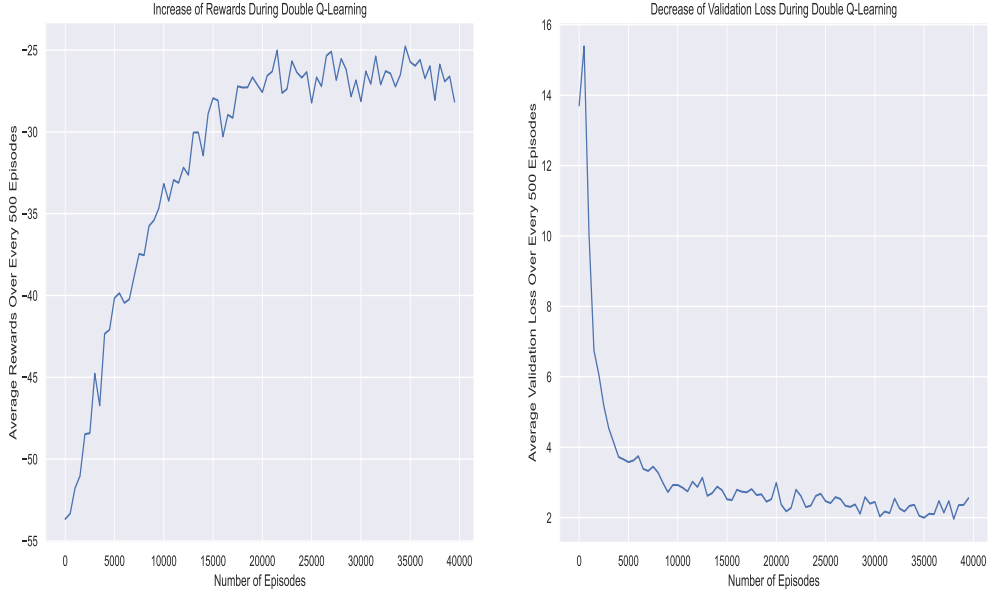


Figure 8: Training Dynamics for the Simulation Experiment in Section 5.1

median, and the third quartiles compared to those of the oracle distribution, respectively. The quartiles of each posterior distribution is computed via 1,000 independent draws. In all these figures, we observe similar superior performances for the MI, Max Var, and the Q-learning methods over the EAP and the MAX pos approaches in estimating the entire oracle distributions. Consistent with the findings in Section 6.1, the Q-learning approach demonstrates the fastest error reduction rate, especially in the early stages of the test.

## F DESE Educational Assessment

Our analysis for the DESE education dataset closely aligns with the analysis in [1]. However in [1], the authors demonstrated the effectiveness of the PXL-EM algorithm in estimating interpretable factor loadings and the true number of factors using Grade 10 DESE data. In this work, we focus on Grade 8 data since it contains slightly larger number of items.

We adopted the idea of dynamic posterior exploration, letting the regularization  $\lambda_0$  parameter in the PXL-EM algorithm to gradually increase over the path  $\{1, 5, 10, 20, 40, 60, 80, 100\}$ . The resulting factor loading matrix  $B$  is visualized in Figure 12, where dark blue regions indicate exact zeros. Notably, all English items load exclusively onto the first factor, representing general ability, while math items can also load onto factors 2–4, reflecting

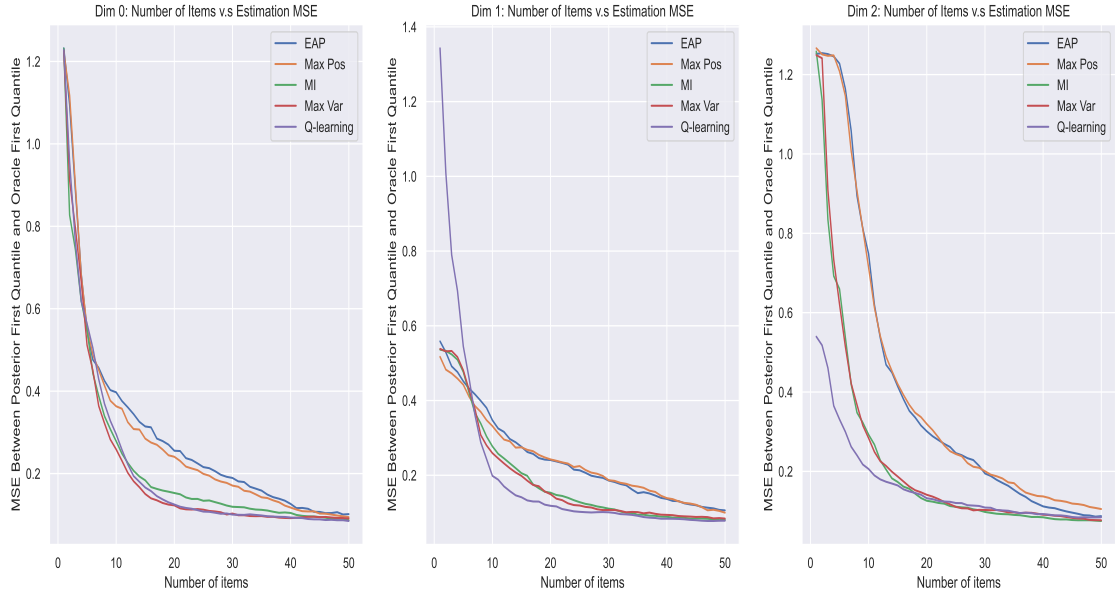


Figure 9: MSE Between Posterior 1st Quantile and Oracle 1st Quantile

their greater structural complexity. For instance, the final factor (“Math 3”) has nonzero loadings only on items 34, 36, and 38, all of which correspond to geometry problems.<sup>1</sup> Interestingly, the authors in [1] obtained very similar factor loading matrix estimation for the Grade 10 data as well.

<sup>1</sup>Exam questions are available at: <https://www.doe.mass.edu/mcas/2022/release/>.

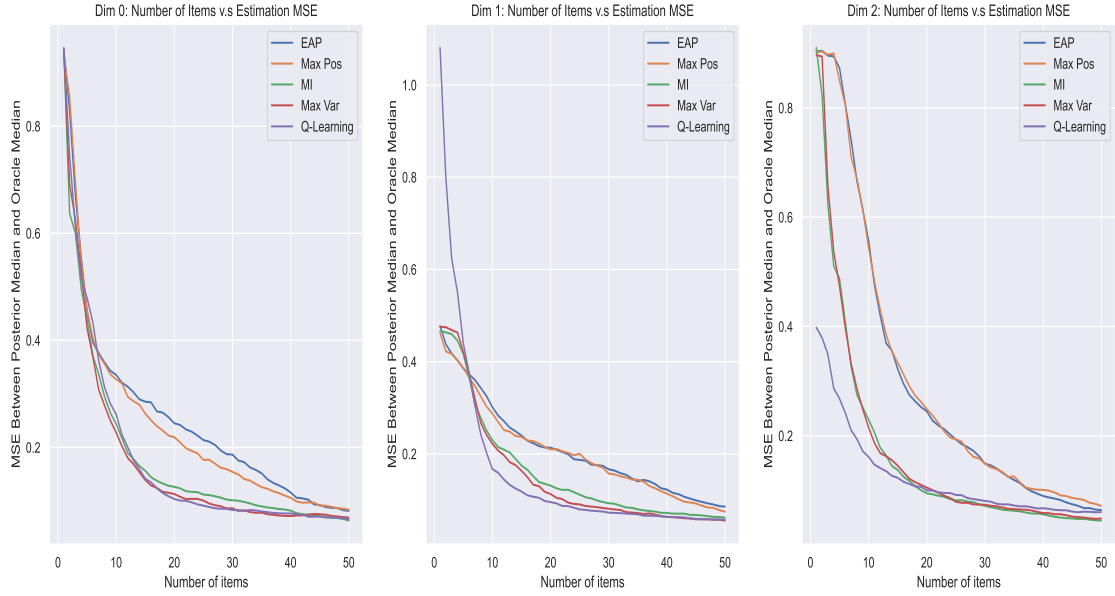


Figure 10: MSE Between Posterior Median and Oracle Median

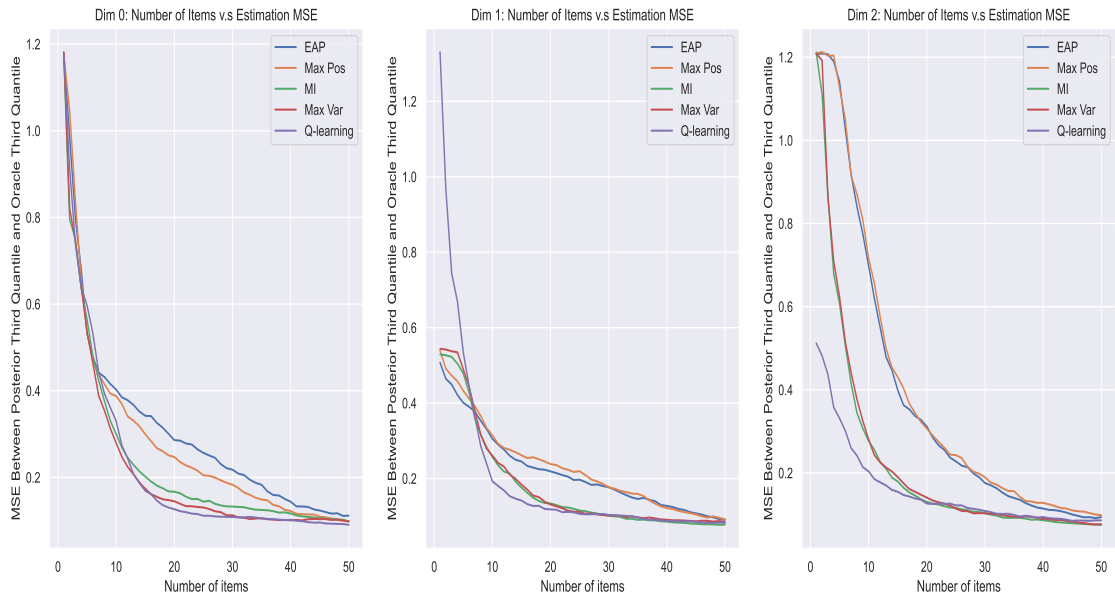


Figure 11: MSE Between Posterior 3rd Quantile and Oracle 3rd Quantile

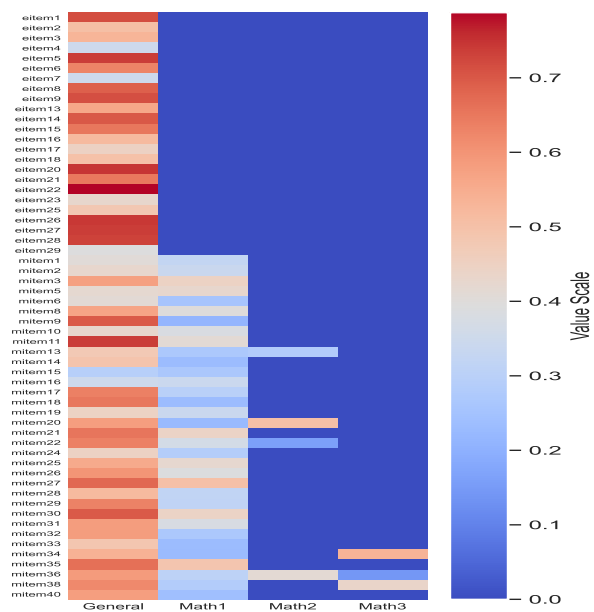


Figure 12: Estimated Factor Loadings for DESE Data